Report
R-17-19
October 2018

Phosphorus in copper intended for spent nuclear fuel disposal

Henrik C. M. Andersson-Östling
Joacim Hagström
Mats Danielsson

SVENSK KÄRNBRÄNSLEHANTERING AB

SWEDISH NUCLEAR FUEL
AND WASTE MANAGEMENT CO

Box 3091, SE-169 03 Solna
Phone +46 8 459 84 00
skb.se

SVENSK KÄRNBRÄNSLEHANTERING

ISSN 1402-3091
SKB R-17-19
ID 1578826
October 2018

Phosphorus in copper intended for spent nuclear fuel disposal

Henrik C. M. Andersson-Östling, Joacim Hagström,
Mats Danielsson

Swerea KIMAB AB

Abstract

The creep behaviour of phosphorus doped copper has been studied. Both mathematical modelling and experimental studies has been used. The results show that phosphorus is evenly distributed within the grains and no widespread segregation of phosphorus to grain boundaries has been found. Studies of the diffusion of the phosphorus atoms in the copper matrix has shown that at temperatures relevant for the repository, no movement of the distributed phosphorus atoms can be expected over the timescale of the repository. Microstructural modelling of the material shows that no recrystallization is expected at the repository temperatures. Taken as a whole, the structure a creep activated dislocation moves through during creep is expected to remain constant during repository temperatures and timescales, hence the creep properties are also expected to remain constant during the same time and the same or lower temperature.

Previous theories regarding dissimilar creep properties in large or small grains has been explained as invalid by microstructural modelling of a virtual bimodal grain structure.

Contents

1 Introduction 7

2 Theoretical background 9
2.1 The SKB disposal method 9
2.2 Phosphorus in copper – theories 10

3 Scientific strategy for the work in this report 13
3.1 Microstructural modelling 13
3.2 Microscopic examinations using SEM and TOF-SIMS 13
3.3 Experimental study 13

4 Microstructural modelling of copper and relaxation experiments 15
4.1 Background for the microstructural modelling 15
4.2 Modelling and relaxation experiments 15
4.3 Results from the relaxation experiments 15
4.3.1 EBSD analysis of Cu-OF and Cu-OFP heat treated at 215 °C 16
4.3.2 EBSD analysis of Cu-OF and Cu-OFP heat treated at 250 °C 16

5 Modelling of grain size distribution 19
5.1 Single crystal copper 19
5.1.1 Elastic behaviour of single crystal FCC materials 19
5.1.2 Inelastic behaviour of single crystal FCC materials 19
5.1.3 Material parameters for single crystal copper 20
5.2 Polycrystal modelling 21
5.2.1 A single grain size distribution 21
5.2.2 A bimodal grain size distribution 22
5.2.3 Initial texture 23
5.2.4 A measure of effective plastic strain 23
5.3 Results 24
5.3.1 Evolution of local effective plastic strain 24
5.3.2 Comparisons of small and large grains with respect to effective plastic strain 25

6 Experimental creep testing 29

7 Metallography 33

8 Results 35
8.1 Creep testing 35
8.2 Metallography creep test specimens 35
8.3 TOF-SIMS 43
8.4 Annealing experiments on Cu-OFP 47

9 Discussion 49
9.1 Microstructural modelling and relaxation experiments 49
9.2 Grain size distribution modelling 49
9.3 Diffusion dynamics in Cu-OFP 49
9.4 Phosphorus distribution in Cu-OFP 49
9.5 Grain boundary stability and recrystallization 50
9.6 Creep in phosphorus containing copper 50
9.7 The role of phosphorus in the creep of Cu-OFP 50
9.8 Questions raised by the work in this report 51

10 Conclusions 53

References 55

1 Introduction

Copper intended for spent nuclear fuel disposal must exhibit a high degree of ductility to fulfil the requirements of the KBS-3 method. The copper is intended to provide corrosion resistance over the period of the repository, which is in excess of 100 000 years. The copper must also have sufficient creep ductility to withstand the initial manufacture of the canisters and the hydrostatic pressure at the repository depth. Initial designs used oxygen free copper, but this was found to have insufficient creep ductility (Andersson-Östling and Sandström 2009). To increase the ductility oxygen free copper has been doped with phosphorus. The role of phosphorus in the creep properties of copper is insufficiently understood. It is known from empirical studies in a short timescale, up to 20 years, that it has a beneficial effect on the creep ductility which increases from less than 5 % to over 50 %. This just by adding as little as 50 wt-ppm phosphorus to oxygen free copper. What is lacking is a scientific understanding as to why it has an effect. Without this fundamental understanding one cannot make the assumption that it will have the same effect over a hundred thousand years, which have been pointed out by the Swedish Radiation Safety Authority (SSM) (SSM 2014).

The work presented in this report aims at developing a scientific understanding through combining advanced modelling on an atomic level, diffusion modelling, constitutive modelling of creep in an idealized grain structure, metallography and analysis of the phosphorus content and distribution in the material. The initial hypothesis tested in the work presented in this report regards the interaction between phosphorus atoms and dislocations in the area of the grain close to the grain boundary. Just not at the interface itself, which has been the predominant view in the scientific community so far. Creep tests performed on phosphorus doped copper in an unrelated investigation (Mannesson and Andersson-Östling 2013) have shown this extended interaction to be a potential explanation, and one that lends itself to experimental verification if studied enough. Over the time of the project the focus area for the work has shifted as new data has been discovered and the direction of the research has therefore changed, and the report describes this change.

2 Theoretical background

2.1 The SKB disposal method

Spent nuclear fuel in Sweden is planned to be disposed of by the KBS-3 method (SKB 2010b). The main idea of this method is to place the fuel rods in a cast iron insert placed within a copper shell. The copper shell is then welded shut. The planned finished canister will finally be placed in a bentonite lined deposition hole deep in the bedrock. The whole repository will consist of approximately 6 000 canisters, and the timescale of the repository is several hundred thousand years. During this time the repository will experience glaciation periods as well as interglacial periods.

During this time the repository will experience several glaciation periods with the accompanying changed stress levels for the canister.

The main idea of the canister is that the cast iron insert will supply mechanical strength, the copper shell corrosion protection to keep the spent nuclear fuel separated from the surrounding groundwater and finally the bentonite clay to provide a barrier to shield the canister from minor movements in the bedrock, but also to hinder the transport of radionuclides in the event of a breach of a canister. During the first time in the repository, perhaps up to a thousand or so years, the surrounding groundwater will saturate the bentonite clay and, due to the special properties of bentonite, this will expand and increase the pressure on the canister until equilibrium is reached where the bentonite can expand no more.

The copper shell is vital to provide corrosion resistance. It must stay intact for the whole of the repository timescale. The copper shell is manufactured by the extrusion of a copper tube followed by a machining stage when the tube is taken down to the final dimensions. The top and bottom lids are forged and machined pieces and they are fixed to the copper tube by friction stir welding. The cast iron insert is placed into the copper tube before the top lid is welded in place, and to ensure a smooth insertion of the cast iron, a radial gap of 1.5 mm is present between the cast iron and the copper tube. This gap will close due to the hydrostatic pressure when the bentonite clay expands as it is saturated by water. The copper will deform to a significant amount during this process and the deformation process could be uneven depending of the saturation of the bentonite clay.

The canister temperature is estimated to be around 100 °C within a few years after being placed in the bentonite due to residual radioactivity in the spent fuel. The temperature will decrease to room temperature (22 °C) over the first 1 000 years and after 5 000 to 10 000 years the temperature will decrease to that of the surrounding rock, 12 °C (SKB 2006). This temperature is high enough to allow the copper to deform by creep instead of short term plastic deformation. No cracks are expected, or allowed, during this stage.

After the initial deformation there will be no more gaps between copper and cast iron, but creep will still be active later in the repository. This could be for instance changes is the stress state around the canister during a glaciation period or an earthquake which could place a shear stress on a canister. The bentonite could also saturate unevenly, leading to excessive bending of the canister. Details on these scenarios can be found in Raiko et al. (2010).

All in all the demands on the mechanical properties of the copper used in the canisters are high. It will have to allow creep at temperatures between 100 and 4 °C and it cannot display cracking tendencies. It will also have to have the same properties after extended periods of time, hundreds of thousands of years. Normal extrapolation methods are not by themselves sufficient. For a standard heat resistant material an extrapolation of an order of magnitude is allowed at the most, 100 years of service for 10 years of maximum experimental test time. This gives a ratio of 1:10. In the case of copper for spent nuclear fuel canisters a ratio of 1:50 000 is needed (100 000 years for a maximum laboratory experiment time of 20 years). Extended extrapolation methods have given an indication that the stresses, strains and deformations expected in the repository is found in Sandström (1999).

This however requires that the physical and chemical properties of the copper remain stable over the whole of the repository timescale. A researcher has voiced doubts of the veracity of this (Pettersson 2012, 2016). Furthermore the Swedish Radiation Safety Authority (SSM) has pointed

to this as a concern regarding the whole KBS-3 design (SSM 2014). The element in the centre of the scientific discussion is phosphorus. When copper was first contemplated for use as a corrosion barrier standard oxygen free copper (Cu-OF) was creep tested and soon the tests exhibited low creep ductility. Examples of this can be found in the review report on copper creep that was released in 2009 (Andersson-Östling and Sandström 2009). Then it was found that in the United States a grade of pressure vessel copper with a small phosphorus addition was used which was known to have higher creep ductility. This was duly tested and it was found that an addition of 50 ppm phosphorus to the previously used Cu-OF increased the creep ductility from 2–3 % to 50–60 %. The new grade of copper is known as Cu-OFP where P stands for phosphorus. At the present time a huge amount of creep tests has been conducted and none has shown low ductility tendencies (Andersson-Östling and Sandström 2009).

What is lacking is a scientific explanation of what phosphorus actually does on an atomic level in the copper, and why it has a beneficial effect. Here the dissenting researcher must be acknowledged. His arguments can be condensed into one question. "We know that phosphorus has an effect in the short term, but can we really be sure that the beneficial effect lasts the whole time of the repository, or will the Cu-OFP after an extended time revert to the creep properties of Cu-OF and crack?" This is the critical question and no one has so far come up with an acceptable answer to the fundamental question. Several theories have been proposed but none has been able to prove experimentally unequivocally. The most recent attempt has in strong terms and with theoretical arguments shown that it is most probable that the effect is long lasting (Sandström 2014). But the question remains.

2.2 Phosphorus in copper – theories

In the literature only few theories on the fundamental role of phosphorus in copper has been published. One published work concerns the way phosphorus interacts with sulphur in a copper matrix (Korzhavyi et al. 1999). Sulphur is an unwanted alloying element in copper and effort is taken during the processing of the copper to minimise the sulphur content. Some always stays in the matrix and a normal low content of sulphur is below the SKB limit of 12 wt-ppm. The idea in this work is that phosphorus and sulphur competes for the same substitutional sites in the unit cell. Sulphur is known to cause brittleness in copper, and if sufficient phosphorus is present in the matrix the preferred sulphur sites is populated by phosphorus and hence the brittleness is eliminated. The theory, which is fundamentally sound, does however have some unresolved issues. Sulphur is traditionally thought of as embritteling the grain boundaries since sulphur has been detected on the fracture surfaces, but no phosphorus has been found in the same way. Also, both sulphur and phosphorus are substitutional atoms in the matrix, and the sulphur has to go somewhere in the matrix, meaning that the embritteling effect would just be ameliorated by phosphorus, not eliminated which experiments show. A recent study has shown how phosphorus, sulphur, hydrogen and oxygen could interact in the copper (Magnusson and Frisk 2014). The process is complex and several compounds between the constituents can form.

Recent research in a largely unrelated investigation has shown new evidence which might be interpreted as an effect of phosphorus. In this work copper, which during post manufacturing NDT ultrasound showed higher than normal sound attenuation, was creep tested at 75 °C (Mannesson and Andersson-Östling 2013). The sound attenuation is, given that all other factors are kept constant, a direct effect of the grain size and distribution. Two of the images from this project are given in Figure 2-1 and Figure 2-2. While not a part of the work in this investigation the rather peculiar appearance of the grain structure before and after creep testing was noted. Before testing the grain distribution was consisting of rather large grains, ca 500 µm, in a matrix of rather smaller grains ca 100 µm. After testing, a similar structure was observed near the necking part of the test specimen. In this area all of the smaller grains had taken on an elongated appearance, but the larger grains exhibited less deformation, Figure 2-2.

Normally this is not seen in creep test specimens. For a structure of mixed grains with similar creep properties, as this copper have, all grains should deform equally. The copper chemical composition is known. The oxygen content is 3.2 ppm, the sulphur content around 5 ppm and the phosphorus content close to 40 ppm. The deformation state and hence the dislocation density is also thought to be roughly similar throughout the material in the specimen. Temperature gradients, which might affect the dislocation movement rate, are not present since the heating is uniform in the specimen.

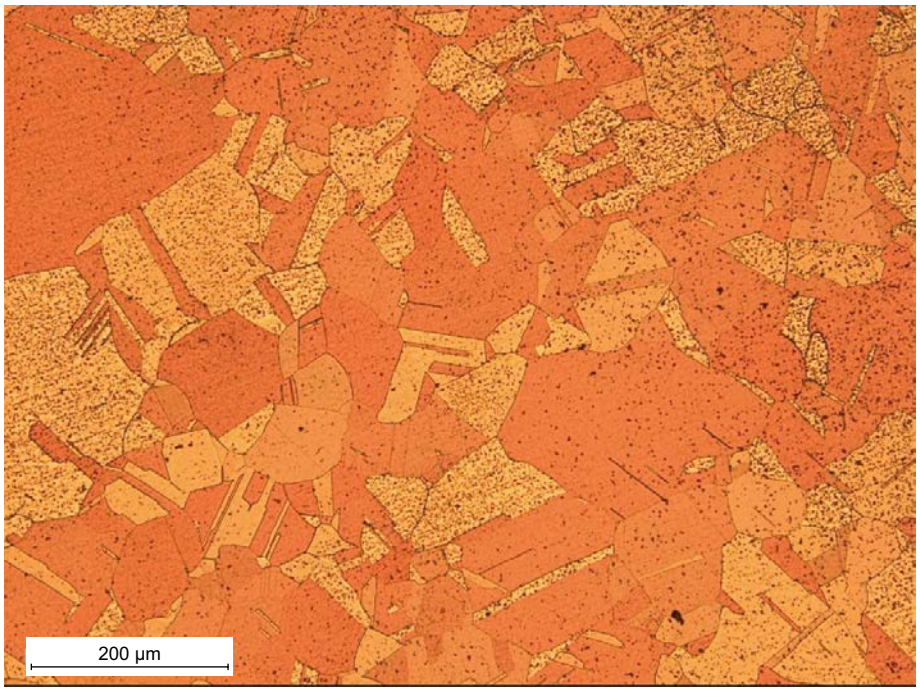

Figure 2-1. *Microstructure before creep testing consisting of a mixture of large and small grains.*

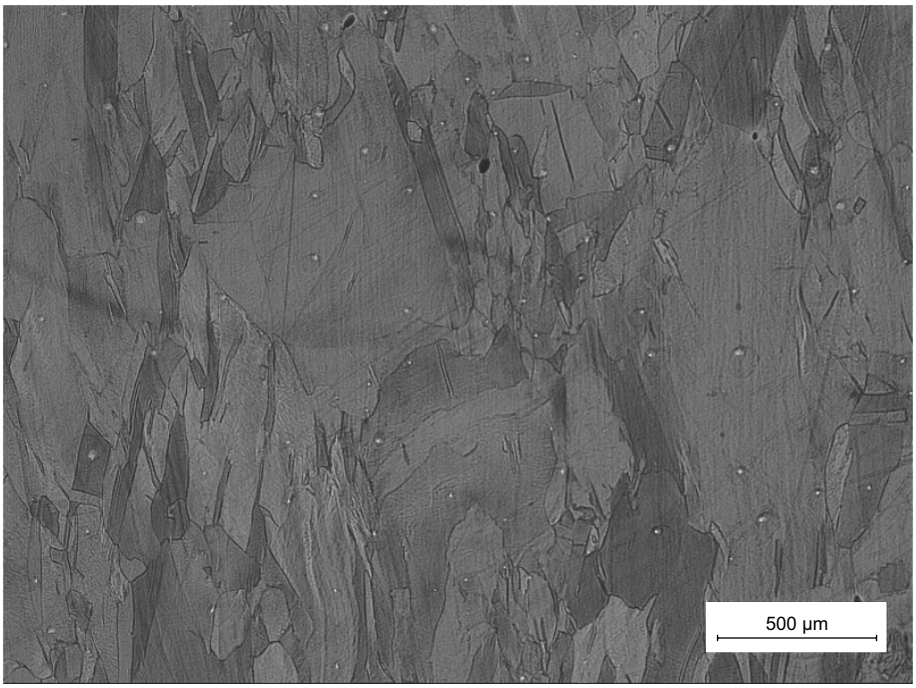

Figure 2-2. *Similar microstructure as in Figure 2-1 after creep testing. Note the elongated appearance of the smaller grains compared to the more fixed appearance of the larger grains.*

3 Scientific strategy for the work in this report

3.1 Microstructural modelling

The work in this part will aim at developing a randomised grain structure model. The model will give the possibility to use different creep models and constitutive equations in different parts of the same grain. The model will also consist of several individual grains with different sizes and orientations. The modelling will be performed in 2-D and 3-D. Using the model, with the input given by the other parts of the work, it will be possible to model the development of creep in a grain structure. The results can then be compared to practical creep experiments to verify the theoretical mechanism.

Studies of the relaxation behaviour will also be a part of the modelling work. In this part simple experiments will be performed on Cu-OFP and Cu-OF to study the recrystallization behaviour at temperatures around 250 °C.

3.2 Microscopic examinations using SEM and TOF-SIMS

In the past it has been impossible to study any segregation of phosphorus, sulphur and oxygen since all signals in microprobe, ASEM (Analytical Secondary Electron Microscopy) and backscatter SEM has been "drowned" by the copper signal. Sulphur has been detected on the fracture surface of ruptured creep specimens, but no sulphur structure has been identified inside the grains. Bulk content has always been possible to study though. The aim of this part of the work is to use the newly developed and improved methods available today. Especially TOF-SIMS (Time-Of-Flight – Secondary Ion Mass Spectroscopy) will be used to study actual copper grains both from extruded, machined, heat treated and creep tested material. Any phosphorus and sulphur segregations, and the concentration level will be identified. General references for the use of TOF-SIMS can be found in Benninghoven (1994) and two papers from VanVaeck and Adriaens et al. (Van Vaeck et al. 1999, Adriaens et al. 1999).

3.3 Experimental study

The experimental study will aim at proving the modelling results. Different microstructures, extruded as well as forged material and weld metal, will be creep tested at temperatures around 75 °C. The tests will not be allowed to rupture but instead they will be stopped at set creep strains and then studied metallographically. The experimental work will also provide model materials for all other parts of the work.

4 Microstructural modelling of copper and relaxation experiments

4.1 Background for the microstructural modelling

Henderson and Sandström (1998) creep tested various batches of oxygen-free, high conductivity copper at temperatures ranging from 75 to 245 °C. Some batches displayed alarmingly low levels of creep strains to rupture at temperatures in excess of 180 °C. Fractographic analyses suggested that specimens failed in an intercrystalline manner. Subsequent comparisons of oxygen free copper (Cu-OF) and phosphorus-alloyed copper (Cu-OFP) have suggested that the addition of 50 ppm phosphorus suppresses the previously observed drop in ductility at higher temperatures; see Andersson-Östling and Sandström (2009, Figure 8-3). Cu-OFP is now the copper alloy that SKB has chosen for the canisters meant for disposal of spent nuclear fuel using the KBS-3 concept. In addition to suppressing brittle fracture, the addition of phosphorus has been shown to significantly decrease the rate of deformation of Cu-OFP in load-controlled so-called creep tests when compared to Cu-OF. To this day, the underlying reasons are unclear for why the addition of phosphorus seems to be beneficial to the mechanical behaviour of copper. In this report, it is investigated whether Cu-OF and Cu-OFP behave differently with respect to recrystallization. The experimental program is outlined in the next section.

4.2 Modelling and relaxation experiments

The purpose of the study is to examine the relative tendency for recrystallization of Cu-OF and Cu-OFP. Of particular interest are the temperatures at which Cu-OF was shown to display poor ductility in the study by Henderson and Sandström (1998). Cold work increases the tendency for recrystallization, and the two materials are therefore subjected to a controlled level of cold work prior to exposure to high temperatures. The experimental program is as follows:

1. Manufacturing of tensile test specimens of Cu-OF and Cu-OFP.
2. Annealing of the specimens to remove the effects of cold work introduced when manufacturing.
3. EBSD (Electron BackScatter Diffraction) analyses on electro-polished samples of then-discarded specimens to ensure success in the previous step.
4. Tensile testing of both materials at room temperature to an axial (engineering) strain of 20 %.
5. Extraction of small samples from the tensile specimens.
6. Heat treatment of both materials at different temperatures:
   a. 215 °C for three weeks.
   b. 250 °C for three weeks.
7. Electro-polishing of the samples and EBSD analyses to search for signs of recrystallization.

4.3 Results from the relaxation experiments

A study of recrystallization is performed using EBSD on samples from the cold-worked and subsequently heat treated tensile specimens. Grains that are not recrystallized are expected to show non-uniform crystallographic orientations due to the previously induced cold work. On the other hand, a recrystallized grain is expected to show uniform crystallographic orientation because it will have formed with no subsequent cold working.

In the EBSD charts that are shown in the sections to follow, the grain mean orientation deviation is shown. It is a measure that considers each grain separately. It plots the deviation in crystallographic orientation at each sampled point in the grain from the grain *mean* orientation. In a completely recrystallized grain, i.e. a grain with a uniform orientation, the deviation from the mean will be zero everywhere, producing a solid blue grain in a chart.

4.3.1 EBSD analysis of Cu-OF and Cu-OFP heat treated at 215 °C

Figure 4-1 shows the grain mean orientation deviation for the case of cold worked Cu-OF, heat treated at 215 °C. As indicated by the arrows in the image, some grains have recrystallized as a consequence of the cold work and heat treatment.

Figure 4-2 shows the grain mean orientation deviation for the case of cold worked Cu-OFP, heat treated at 215 °C. The Cu-OFP samples displayed no signs of recrystallization.

4.3.2 EBSD analysis of Cu-OF and Cu-OFP heat treated at 250 °C

Results shown in the previous section demonstrated that the phosphorus-alloyed OFP copper appears more stable against recrystallization, whereas Cu-OF shows signs of partial recrystallization when heat treated at 215 °C. In this section, analogous results are shown for the higher temperature of 250 °C. Figure 4-3 shows the grain mean orientation deviation for Cu-OF. When heat treated at 250 °C, the signs of recrystallization become more pronounced. Several grains have now recrystallized, as indicated by the arrows in the figure.

Figure 4-4 shows the case of Cu-OFP heat treated at 250 °C. The EBSD chart of grain mean orientation deviation offers no sign of recrystallization. Again Cu-OFP appears to be more stable against recrystallization than Cu-OF.

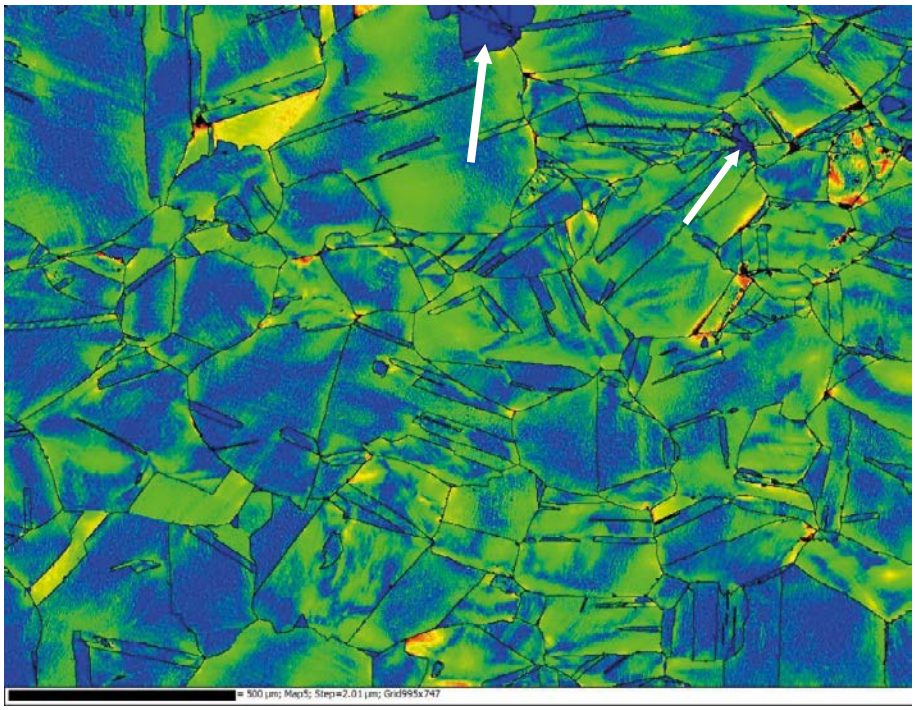

Figure 4-1. *Grain mean orientation deviation of Cu-OF, heat treated at 215 °C.*

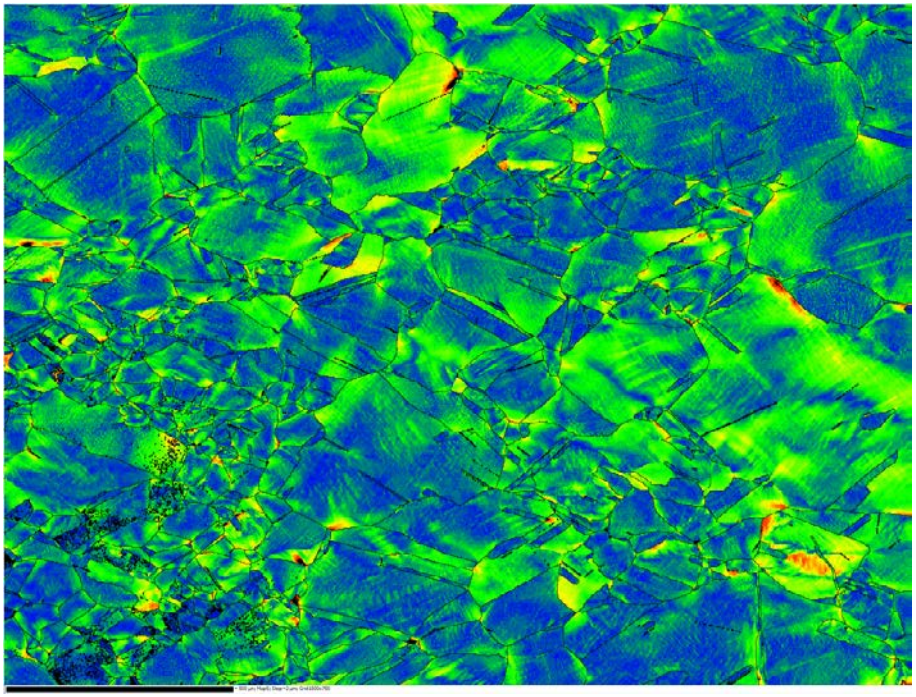

Figure 4-2. *Grain mean orientation deviation of Cu-OFP, heat treated at 215 °C.*

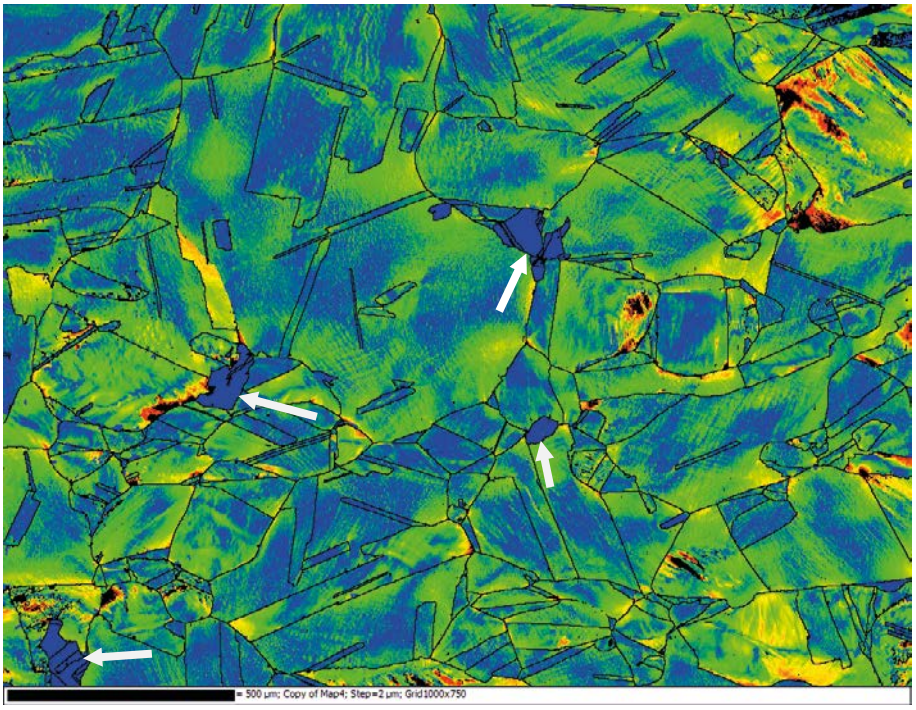

Figure 4-3. *Grain mean orientation deviation of Cu-OF, heat treated at 250 °C.*

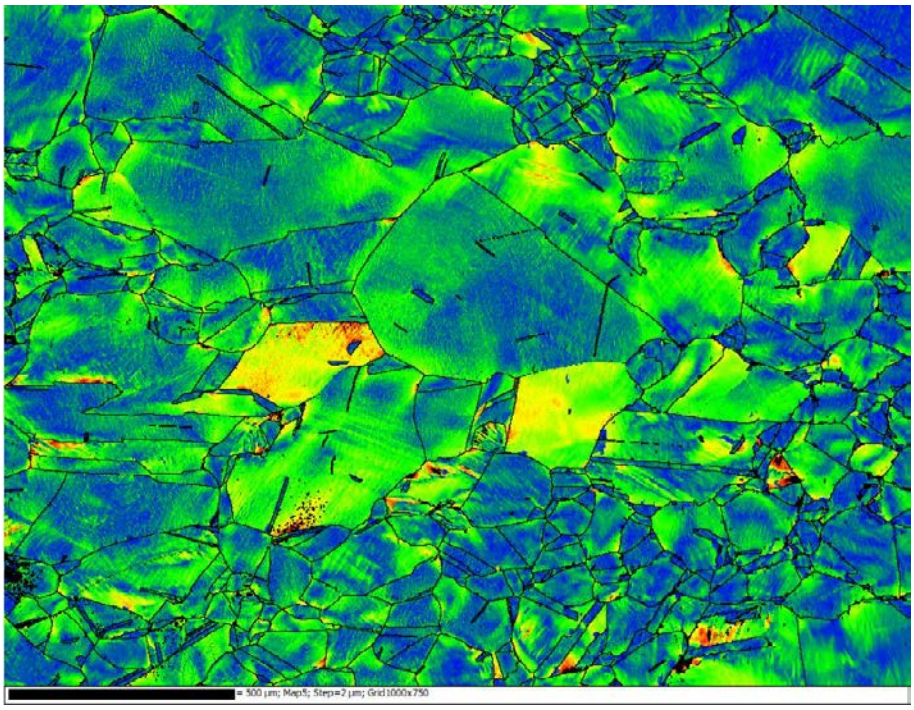

Figure 4-4. *Grain mean orientation deviation of Cu-OFP, heat treated at 250 °C.*

5 Modelling of grain size distribution

This part of the project concerns microstructural modelling of the polycrystalline microstructure of Cu-OFP, with the particular emphasis of investigating the effect of a bimodal grain size distribution on the local deformations in the material. In the present report, microstructural polycrystalline models have been constructed for finite element method analyses using crystal plasticity mesh generation software, and a single crystal constitutive model for copper has been implemented into a commercial finite element program.

5.1 Single crystal copper

In order to simulate a polycrystalline microstructure, the constitutive behaviour of single crystals must be modelled. In this work, a constitutive model according to Kalidindi (1992) is used. The model describes the large strain, rate dependent mechanical behaviour of FCC materials. Below, the key constitutive equations describing the flow of single crystals are presented. A full description of the constitutive model phrased in a context of large strain kinematics is not given in this report. For full details, see Kalidindi (1992). The model was implemented into the commercial finite element program ABAQUS (2014).

5.1.1 Elastic behaviour of single crystal FCC materials

As an FCC material displays cubic symmetry at the single crystal level, the linear elastic response at this level is given by three elastic constants. These are defined in the current model using the standard constants for cubic elasticity, C_{11}, C_{12} and C_{44}.

5.1.2 Inelastic behaviour of single crystal FCC materials

In an FCC crystal, there are twelve directions in which the crystal may slip. These twelve crystallographic slip directions are called slip systems α. Figure 5-1 illustrates the twelve slip systems of an FCC single crystal. Each slip system is defined by a slip plane and a direction of slip in that plane.

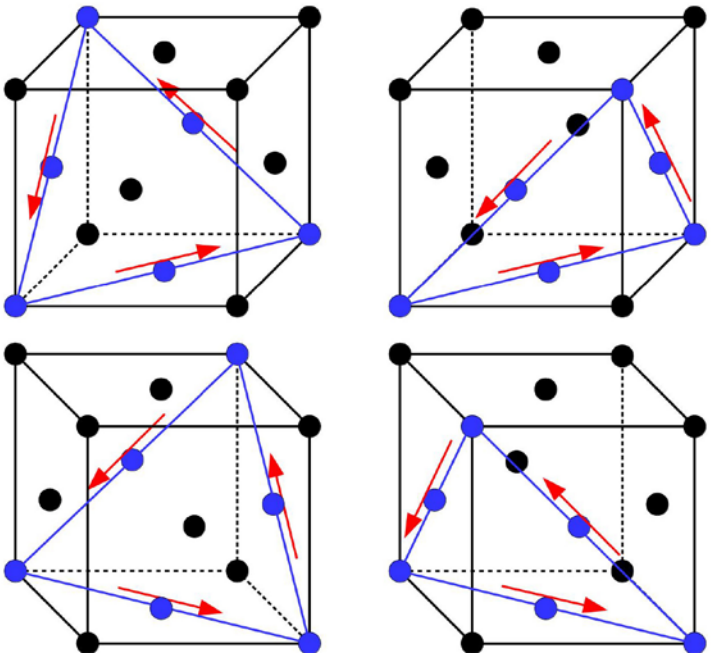

Figure 5-1. *The twelve {111}<110> slip systems of an FCC single crystal. The four slip planes are indicated in blue, and the slip directions in red. Each unit cube represents a set of three co-planar slip directions.*

The flow behaviour of the single crystal is defined at a per-slip-system level. The shear strain rate $\dot{\gamma}^{\alpha}$ of a slip system α is given by a power-law relationship of the form

$$\dot{\gamma}^{\alpha} = \dot{\gamma}_0 \left(\frac{|\tau^{\alpha}|}{s^{\alpha}}\right)^{1/m} \cdot sign(\tau^{\alpha}) \tag{5-1}$$

where $\dot{\gamma}_0$ is a reference shear strain rate, τ^{α} is the shear stress acting on the slip system, s^{α} is the slip system resistance to flow, m is a power-law exponent, and $sign(\tau^{\alpha})$denotes the arithmetic sign of τ^{α}. The evolution of the slip system resistance to flow, i.e. the slip system hardening, is given by

$$\dot{s}^{\alpha} = h^{\alpha\beta}\left|\dot{\gamma}^{\beta}\right|, \ sum\ on\ \beta \tag{5-2}$$

where $h^{\alpha\beta}$ is a hardening matrix and $\dot{\gamma}^{\beta}$ is the shear strain rate on a slip system β. Thus, the hardening of a slip system α is in general affected by slip on all twelve slip systems. The hardening matrix is given by

$$h^{\alpha\beta} = q^{\alpha\beta}h^{\beta}, \ no\ sum\ on\ \beta \tag{5-3}$$

where $q^{\alpha\beta}$ is expressed on matrix form as

$$\boldsymbol{q} = \begin{bmatrix} \boldsymbol{A} & q\boldsymbol{A} & q\boldsymbol{A} & q\boldsymbol{A} \\ q\boldsymbol{A} & \boldsymbol{A} & q\boldsymbol{A} & q\boldsymbol{A} \\ q\boldsymbol{A} & q\boldsymbol{A} & \boldsymbol{A} & q\boldsymbol{A} \\ q\boldsymbol{A} & q\boldsymbol{A} & q\boldsymbol{A} & \boldsymbol{A} \end{bmatrix} \tag{5-4}$$

and where

$$\boldsymbol{A} = \begin{bmatrix} 1 & 1 & 1 \\ 1 & 1 & 1 \\ 1 & 1 & 1 \end{bmatrix}. \tag{5-5}$$

The parameter q is the ratio between the latent-hardening rate and the self-hardening rate. In Equation (5-4), it is implied that the twelve slip systems are arranged in a way that {1,2,3} are co-planar, as are {4,5,6}, {7,8,9} and {10,11,12}. Thus, the ratio of latent-hardening to self-hardening is unity for co-planar systems, and q otherwise. The hardening function h^{β} is given by

$$h^{\beta} = h_0 \left(1 - \frac{s^{\beta}}{s_s}\right)^{a} \tag{5-6}$$

where h_0 is a hardening constant, s_s is a saturation value for the slip system resistance and α is an exponent.

5.1.3 Material parameters for single crystal copper

The material parameters that are used to describe the single crystal are taken from Kalidindi (1992) and represent the mechanical behaviour of pure copper. Note that the (single crystal) material parameters used by Kalidindi (1992) do not correspond to the (polycrystalline) phosphorus alloyed copper (Cu-OFP) used by SKB. The objective of the present work is to investigate whether small and large grains deform differently with macroscopic deformation, and for this purpose, the material parameters used by Kalidindi (1992) should be adequate. Note also that the material parameters used are representing the single crystal behaviour of copper at room temperature. Most mechanical testing of Cu-OFP has been performed at around 100 °C, but again, with the objective of the present work in mind, the present material parameters should be adequate.

Table 5-1 lists the single crystal material parameters. The notation is consistent with the presentation in Kalidindi (1992).

Table 5-1. Material properties for single crystal copper.

Symbol	Value	Function
C_{11}	170 GPa	Cubic elasticity constant
C_{12}	124 GPa	Cubic elasticity constant
C_{44}	75 GPa	Cubic elasticity constant
$\dot{\gamma}_0$	0.001/s	Reference strain rate
m	0.012	Rate equation constant
q	1.4	Latent-to-self-hardening ratio
h_0	250 MPa	Strain hardening constant
s_0	16 MPa	Initial value for the slip system resistance
s_s	190 MPa	Saturation value for the slip system resistance
α	2.5	Strain hardening exponent

5.2 Polycrystal modelling

The polycrystal meshing software Neper (see Quey et al. 2011) was used to generate the polycrystals in the present work. Simulations of polycrystals using non-linear constitutive models and large strain kinematics require significant computational power. Naturally, 3-D simulations are more computationally cumbersome than 2-D simulations. In order to handle a large number of grains, the simulations were restricted to 2-D plane strain.

5.2.1 A single grain size distribution

The software Neper uses a Voronoi tessellation technique (see Quey et al. 2011) to generate, in 2-D or in 3-D, models of a polycrystalline microstructure. In its simplest form, the software produces a Voronoi diagram based on a random distribution of seeds. This method is used in this work to generate a polycrystal that uses a single grain size distribution. Figure 5-2 shows the polycrystal that was generated using Neper. It contains 8 000 grains. The model was discretised using finite elements. A small section of the meshed polycrystal is shown in Figure 5-3. The entire polycrystal consists of 377 605 second order triangular plane strain elements, and 756 780 nodes.

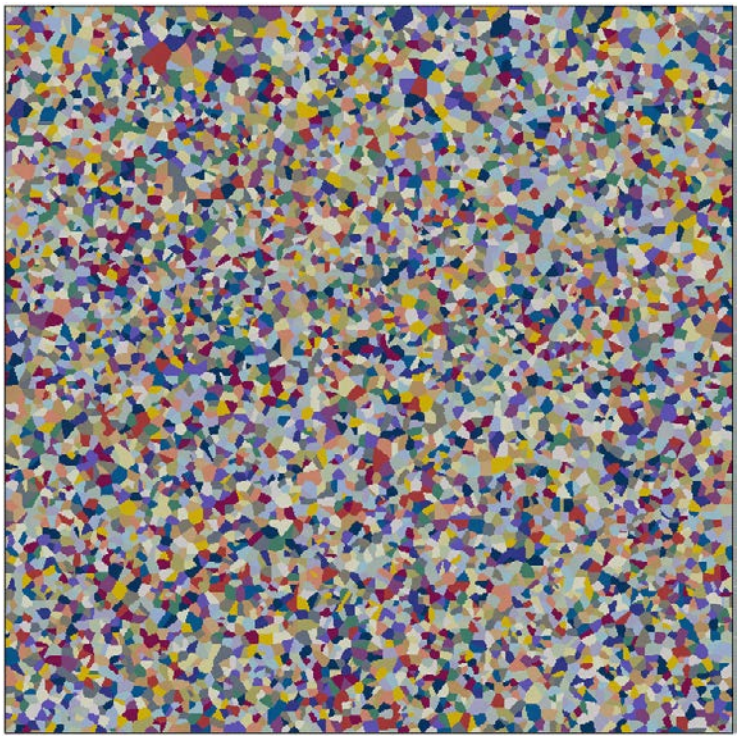

Figure 5-2. *The polycrystal using a single grain size distribution.*

Figure 5-3. *A small section of the finite element mesh of the polycrystal using a single grain size distribution.*

5.2.2 A bimodal grain size distribution

Several different probability distributions can be used to generate so-called Laguerre tessellations, in which distributions of grain sizes can be obtained. These tessellations are related to ordinary Voronoi tessellations, but differ in that they allow for the randomly distributed seeds to carry different weights. For details, see the Neper documentation (Quey 2014). In this work, a Bernoulli-type distribution was used to generate a bimodal grain size distribution. It was found that the software Neper is very unstable for this application, and several attempts had to be made to generate a polycrystal model. Figure 5-4 shows the polycrystal. There are 8 000 grains in total, of which 71 are about ten times larger than the small grains, by area. Figure 5-5 shows a small section of the finite element representation of the polycrystal. The finite element model contains 760 037 nodes and 379 232 second order plane strain triangular elements.

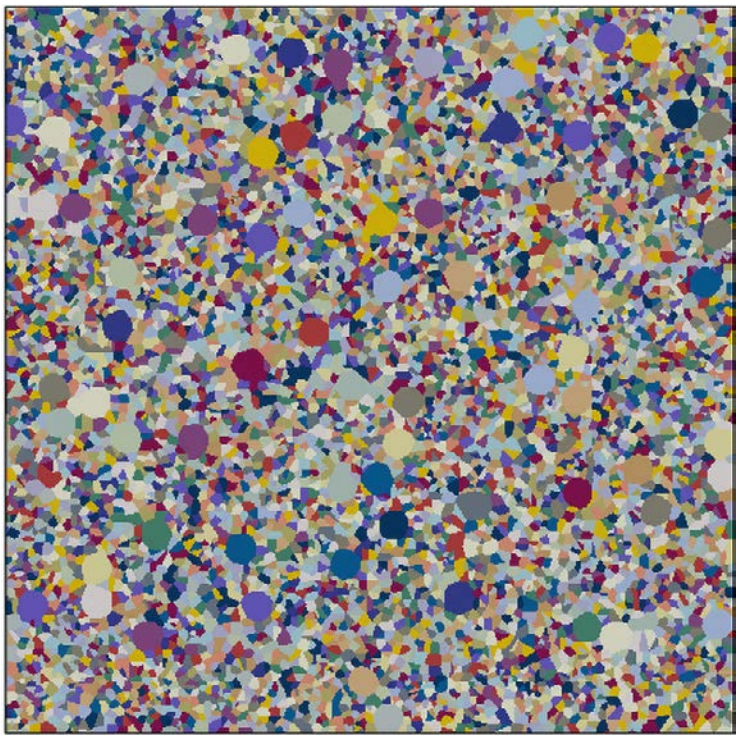

Figure 5-4. *The polycrystal using a bimodal grain size distribution.*

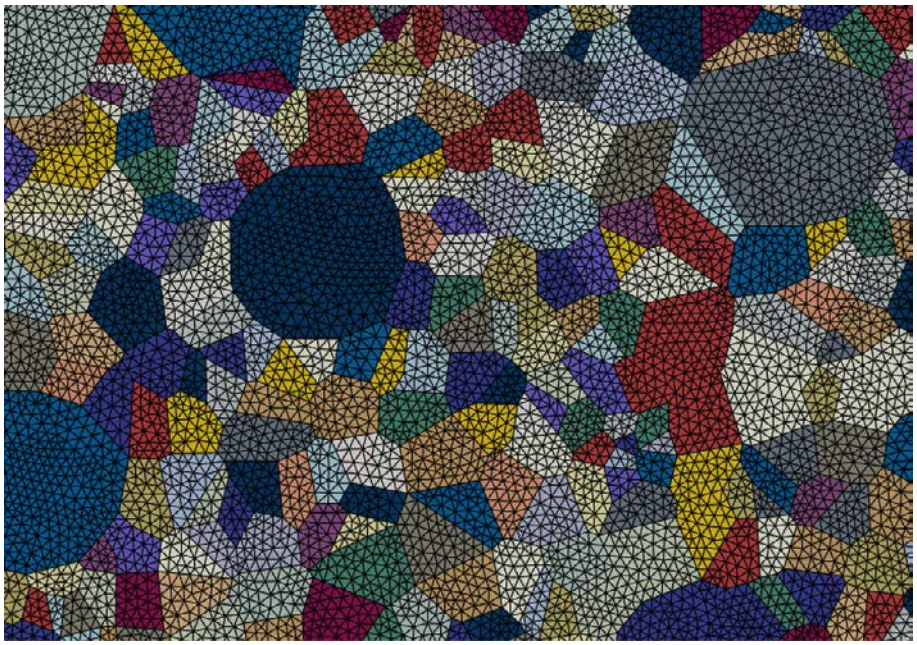

Figure 5-5. *A small section of the finite element mesh of the polycrystal using a bimodal grain size distribution.*

5.2.3 Initial texture

Both polycrystal models discussed previously are assigned an initial crystallographic texture corresponding to an initially isotropic material.

5.2.4 A measure of effective plastic strain

The twelve slip systems in a grain are active depending upon the resolved shear stress acting on each system at a given point in time. Depending on the stress that the grain is subjected to, the number of active slip systems may thus vary with time and it may also vary with the amount of previous strain hardening. There is no obvious way to translate the accumulated shearing of a single crystal into an accumulated, effective value, and consequently, constructed measures of accumulated shear may not be easily interpreted. Rather than explicitly considering the individual slip systems of a deforming single crystal, an effective plastic strain can be defined using the material-point-level plastic strain rate tensor. The large-strain equivalent of the plastic strain rate tensor is the plastic velocity gradient whose symmetric part is the plastic rate of deformation tensor. See Gurtin et al. (2010) for a treatise on both small and large strain deformations of single crystals. The components of the plastic rate of deformation tensor are given by D_{ij}^{p}. The plastic rate of deformation tensor is used to define an effective strain rate increment, which is integrated over time to give the effective plastic strain:

$$\varepsilon_{eff}^{p} = \int_0^t \left(\frac{2}{3} D_{ij}^{p} D_{ij}^{p}\right)^{1/2} dt \qquad (5\text{-}7)$$

The quantity above is used to characterise the local deformation of the polycrystals.

5.3 Results

In this section, the results from the polycrystal simulations are presented. First, the local deformations of the polycrystal with a single grain size distribution are compared to those of the polycrystal with a bimodal grain size distribution. Second, a more methodical approach of studying local deformations is used in which the local deformations of small and large grains are compared.

5.3.1 Evolution of local effective plastic strain

In the plane strain tension simulations, the polycrystal models were deformed to 20 % macroscopic axial strain. The distribution of effective plastic strain in the polycrystal with a single grain size distribution is shown in Figure 5-6.

The figure shows that the macroscopic deformation of the material is due to very inhomogeneous deformation at the grain level (apparent shear banding, and consequently heterogeneous plastic straining). The deformation is shown to have localised into diagonally running shear bands with higher levels of effective plastic strain than their surroundings. The reason for this behaviour is that when the polycrystal is subjected to a state of macroscopic strain, the stress that each individual grain experiences will depend upon the crystal orientation of the grain. In some regions, grains are oriented favourably with respect to the macroscopic conditions since resulting shear stresses on some slip systems become high. In other regions, the grains resist plastic deformation because the resolved shear stresses on the available slip systems are too low. In Figure 5-7, the corresponding information is visualised for the polycrystal having a bimodal grain size distribution. Two example regions containing large grains are indicated by red circles.

Overall, the localisation of plastic straining into diagonally running shear bands is similar to Figure 5-6. However, the red circles in the figure indicate that some large grains appear to deform less than their surroundings. Figure 5-8 shows the deformed polycrystal where the large grains are clearly visible. The two example regions of large grains in Figure 5-7 are indicated also in Figure 5-8.

It is interesting to examine the population of large grains more closely to see if there is a general tendency for large grains to deform less than small grains in a bimodal grain structure. This is the subject of the next section.

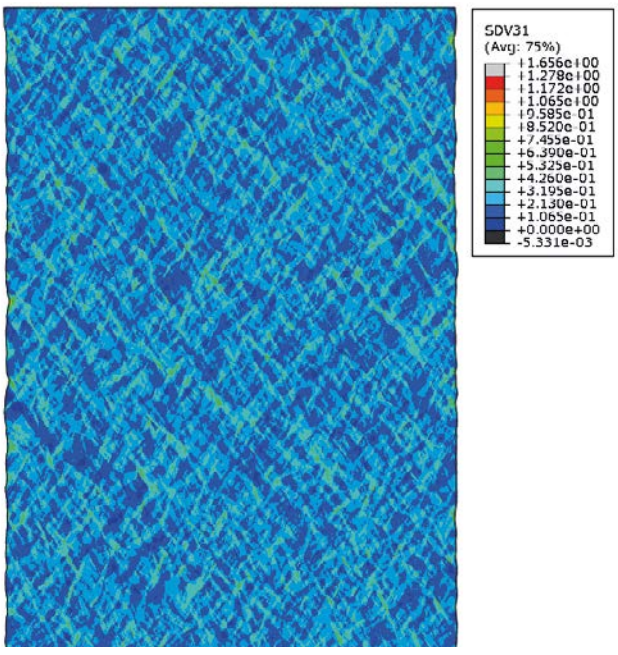

Figure 5-6. *Effective plastic strain in the polycrystal having a single grain size distribution.*

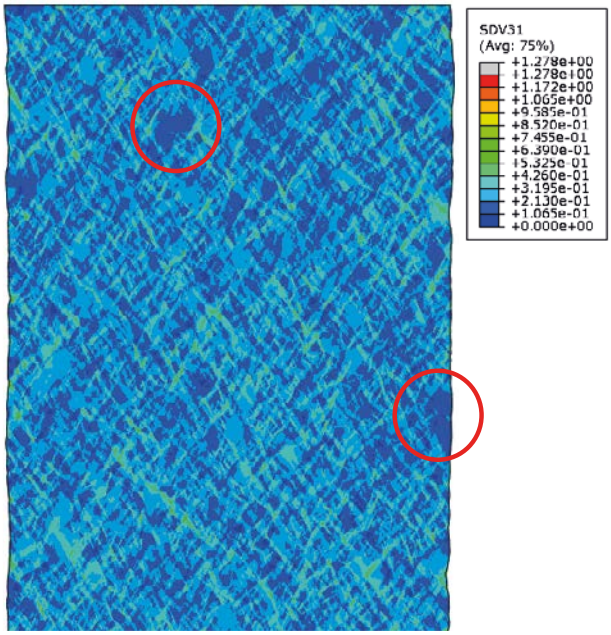

Figure 5-7. *Effective plastic strain in the polycrystal having a bimodal grain size distribution.*

Figure 5-8. *The deformed polycrystal having a bimodal grain size distribution.*

5.3.2 Comparisons of small and large grains with respect to effective plastic strain

In the polycrystal model using a bimodal grain size distribution, it is of interest to investigate how much of the volume average effective plastic strain that is due to deformation of the populations of small and large grains, respectively.

The macroscopic deformation of a polycrystal is due to the accumulated shearing of various slip systems in the individual grains making up the polycrystal. In Equation (5-7), these slip contributions were lumped into a single measure of effective plastic strain. Using the effective plastic strain, a polycrystal volume (or area, in 2-D) average of this measure can be defined as

$$\bar{\varepsilon}^{p}_{eff} = \frac{1}{V}\int_{V} \varepsilon^{p}_{eff}\, dV. \qquad (5\text{-}8)$$

The above measure can also be used to investigate the effective plastic strain in the respective grain size populations. Two additional measures are thus introduced:

$$\bar{\varepsilon}^p_{small} = \frac{1}{V_{small}} \int_{V_{small}} \varepsilon^p_{eff}\, dV, \tag{5-9}$$

$$\bar{\varepsilon}^p_{large} = \frac{1}{V_{large}} \int_{V_{large}} \varepsilon^p_{eff}\, dV. \tag{5-10}$$

Equation (5-9) and Equation (5-10) define the volume average plastic strain in the population of small grains and in the population of large grains. For the polycrystal model using a bimodal grain size distribution, the effective plastic strain of the two grain size populations are normalised by the volume average of the entire polycrystal, giving

$$\frac{\bar{\varepsilon}^p_{small}}{\bar{\varepsilon}^p_{eff}} = 0.998 \tag{5-11}$$

and

$$\frac{\bar{\varepsilon}^p_{large}}{\bar{\varepsilon}^p_{eff}} = 1.022. \tag{5-12}$$

As was mentioned in the background section of this report it has been theorised that in creep tested Cu-OFP small grains deform more significantly than large grains. However, the results from the modeling do not display a significant difference between the deformation of small and large grains. Moreover, in a real polycrystalline material, it is reasonable to expect small grains to be harder (higher resistance to plastic deformation) than large grains due to the Hall-Petch effect. If this grain size effect had been accounted for in the simulation, which it was not, it is likely that large grains would in fact have deformed *more* than small grains. When studying a limited number of micrographs, where only one or very few large grains are contained in a single image, there seems to be a possibility that the large grains could simply be oriented unfavourably with respect to the stress state. This could give a false impression that large grains deform less than small grains. In addition to calculating the average shearing of large grains and relating it to the polycrystal average shearing, the population of large grains was considered in greater detail. Figure 5-9 shows a histogram in which the result in Equation (5-12) is expanded to individual large grains. The figure shows, expectedly, that there is a distribution of deformation about the average deformation of the polycrystal. Some large grains deform more than the average, and some less. It is noted that the grains with the least amount of deformation still deform quite significantly. It is however possible that if one was to examine a domain of grains surrounding a large grain that had deformed much less than the average, a false conclusion could have been drawn suggesting that large grains do not appear to deform compared to small grains.

There could be some question as to comparing simulation results to experimental observations directly, since times and temperatures involved were different. If the tests leading up to Andersson-Östling's observations were performed in such a way that other deformation mechanisms than crystallographic slip were active (such as creep or grain boundary sliding), it is possible that this may offer an explanation.

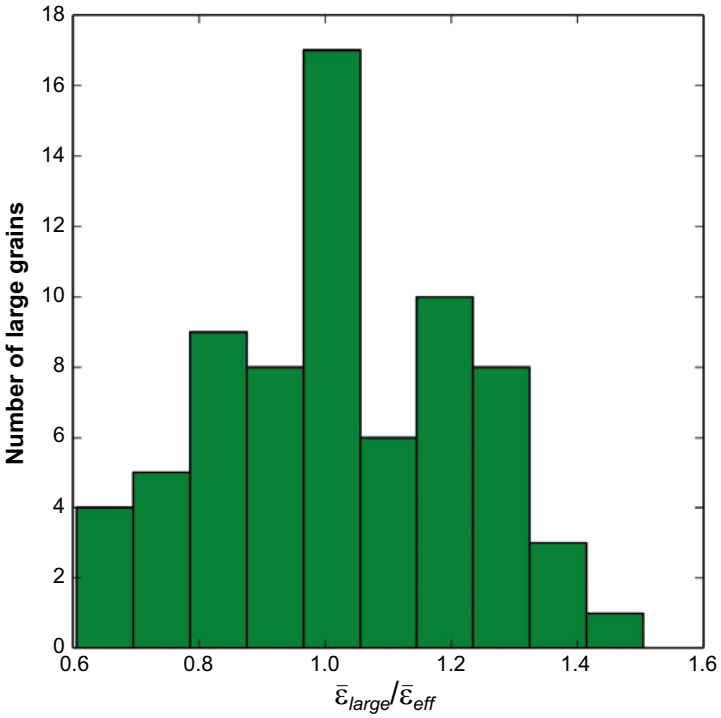

Figure 5-9. *Distribution of deformation in the large-size grain population.*

6 Experimental creep testing

The material used in the investigation is copper from an extruded tube, T58 see also Figure 6-1. The same material has been used for recent studies (Mannesson and Andersson-Östling 2013), Mannesson et al. 2013). The chemical composition can be found in Table 6-1. The creep specimens used can be found in Figure 6-2. The material is annealed (5 minutes at 600 °C in a salt bath, then water quench) before machining and the rectangular shape of the specimen cross section is manufactured by spark erosion (EDM – Electro Discharge Manufacturing) to avoid inadvertently introducing any cold work into the material.

The testing was conducted in the same or similar creep test rigs as in Mannesson et al. (2013) where a full description of the equipment can be found. The test temperature was 75 °C and the test specimens were not allowed to rupture. Instead a test matrix was constructed to allow for interruption after different creep strains.

Figure 6-1. *The material used for the creep testing as delivered. The studies pieces are from the T58 material visible in the upper right corner. The image was taken during the work described in Mannesson and Andersson-Östling (2013).*

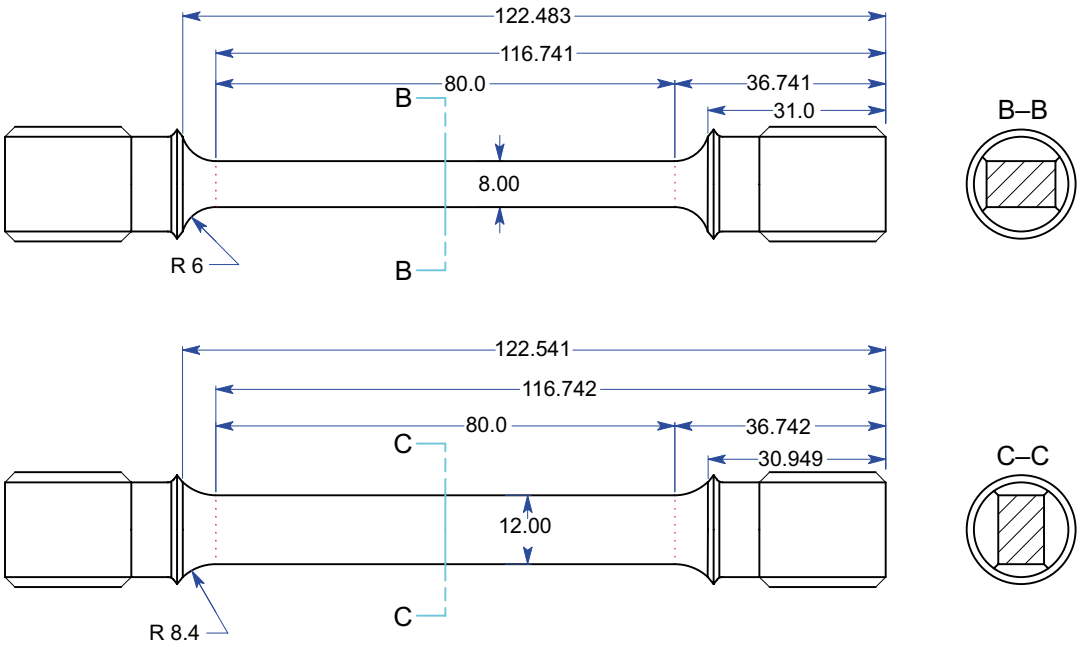

Figure 6-2. *Creep test specimen design.*

Strain was measured using an external extensometer. The measure includes both strain in the specimen and the test rig compliance. The compliance was compensated for as described below. The strain measured on the specimen, $\varepsilon_{total,}$ is made up from four constituents, the thermal strain ε_{th}, the loading strain ε_{load}, the creep strain ε_{creep} and the elastic strain ε_{el}, Equation (6-1). The thermal strain is constant since the testing takes place at constant temperature and the elastic strain is relaxed as soon as the specimen ruptures or is unloaded. The load and the creep strains is exemplified in Figure 6-3 and is made up from the strain measured before full loading of the specimen and the strain measured after full load has been applied.

$$\boldsymbol{\varepsilon_{tot} = \varepsilon_{th} + \varepsilon_{load} + \varepsilon_{creep} + \varepsilon_{el}} \qquad (6\text{-}1)$$

A compensation for the test rig compliance, e.g. the elasticity in the rig, has to be made and has been performed in all cases. The temperature was controlled to within ±1 °C. The test rigs are dynamically controlled by feedback from a loadcell placed in the load train. This feedback is adjusted to a variation of the load of ±3 N, well below the standard requirement of 1 % of the total load. The normal applied load in this work was between 8.5 and 13.5 kN.

Table 6-1. Chemical composition of the material studied in this work. Extruded tube T58. All measurements in wt-ppm. (SKB 2010a).

P	O	S	H	Ag	As	Bi	Cd	Fe
54–56	1.6–2.4	5.3–5.6	<0.1	13.2	0.85–0.87	0.104–0.117	<0.003	1.1–1.2
Mn	**Ni**	**Pb**	**Sb**	**Se**	**Sn**	**Te**	**Zn**	
<0.1	1.1–1.2	0.26–0.29	0.06	0.1–0.2	0.18–0.19	0.05	<0.1	

After creep testing the specimens was cut using a diamond coated cutting disk. The pieces were then sectioned using the same disc axially and mounted in resin. Finally the mounted specimens were polished and etched to reveal the microstructure. A ferrochloric and hydrochloric acid solution recommended for copper was used (Modin and Modin 1985). The cutting of the specimens is described in Figure 6-4. Both light optical, scanning electron microscopy and other analytical methods were used to study the copper.

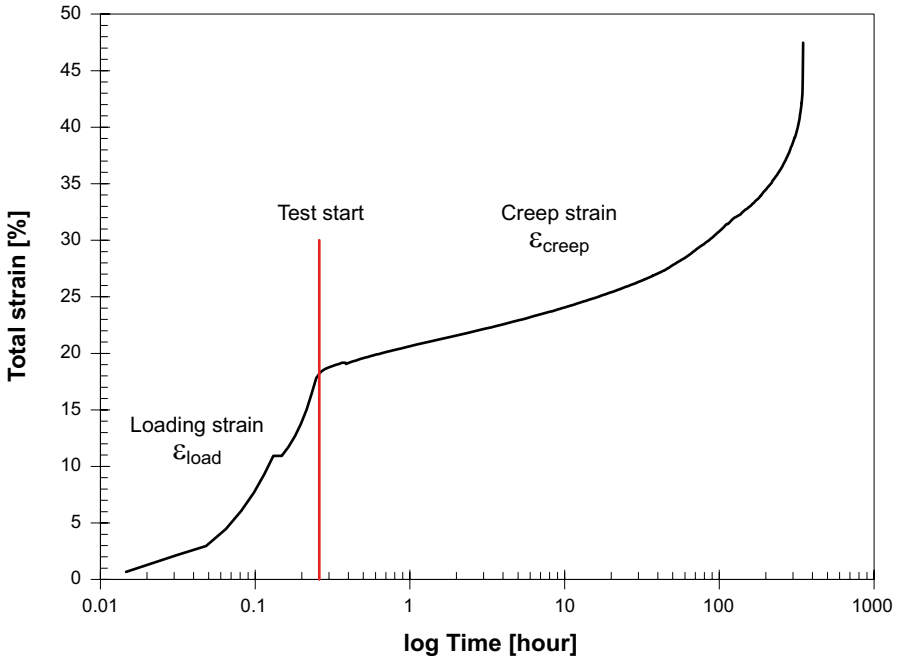

Figure 6-3. *The definition of loading strain, ε_{load}, and creep strain, ε_{creep}*

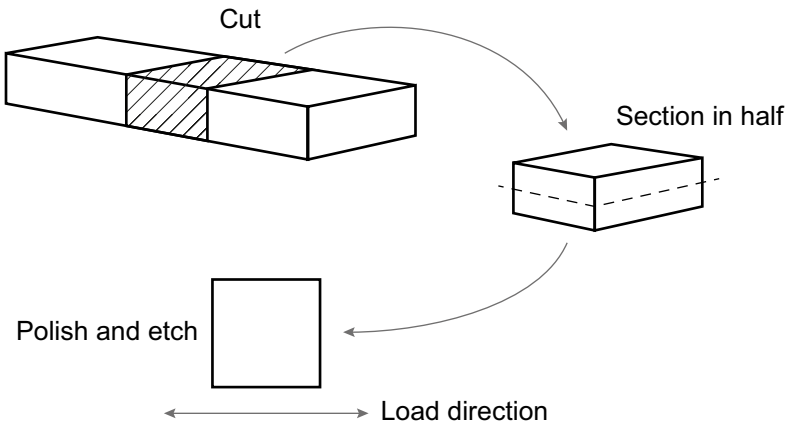

Figure 6-4. *The cutting and polishing of the specimens in the metallographical study.*

7 Metallography

In this study metallography is performed on materials from the creep tests performed within the present investigation as well as materials from other recent investigations. The creep specimens were mainly used to study the grain deformations during creep at different total strains. Both light optical microscopy (LOM) and scanning electron microscopy (SEM) was used on the creep specimens. In the SEM studies EBSD (electron backscatter diffraction) characterisation was used to evaluate crystallographic orientations and misorientations between measurements. Using EBSD deformation can be analysed qualitatively and it can be analysed if deformation occurred localised, eg in deformation bands and in grain boundaries or more homogeneously in the microstructure. Grain boundaries can be analysed and special grain boundaries e.g. twins can be separated from random grain boundaries.

The scanning electron microscope used in the investigation for imaging, EDS and EBSD micro analysis was a LEO 1530 Gemini FEG-SEM. EBSD analysis was conducted using a fast detector (HKL F+) from Oxford Instrument using the acquisition software platform Aztec. Analysis of data was performed using the Channel 5 software package.

Furthermore, TOF-SIMS (Time-Of-Flight – Secondary Ion Mass Spectrometry) was used on annealed and mechanically untested material from previous studies. The main aim for these studies was to evaluate the intra grain segregation, if any, of phosphorus atoms in the copper matrix. The equipment used was a IOFTOF TOF.SIMS5 using Bi_X^+ ions at 25 keV. This work was performed in Germany at Tascon GmbH and in cooperation with the metallurgical department at Swerea KIMAB.

8 Results

8.1 Creep testing

Five creep test specimens were tested at a temperature of 75 °C. The intention was to interrupt the specimens at different total strains. The result from the testing is given in Table 8-1 and an image of the tested specimens in Figure 8-1. By coincidence all of the specimens fall into three groups of similar total strain; 22, 28 and 35 % respectively.

Table 8-1. Creep test matrix, all material from the tube T58.

ID nr	Temp (°C)	Target	Stress (MPa)	Creep time (h)	Loading strain (%)	Creep elong. (%)	Total strain (%)	Min creep rate (%/h)
7	75	10 % creep strain	170	184	12.3	9.97	22.3	0.0237
8	75	5 % creep strain	170	38	18.7	3.97	22.7	–
9	75	rupture	170	148	18.3	17.1	35.4	0.054
10	75	20 % creep strain	170	188	19.2	16.8	36.0	0.0547
11	75	24h creep time	170	24	24.1	4.2	28.3	–

8.2 Metallography creep test specimens

The creep specimens were ground, mounted and polished after which a thorough SEM study was performed with EBSD to identify the crystal orientations. Images from the EBSD study are given in Figure 8-2 through Figure 8-12. In the images the microstructure from the creep tested specimens is represented. The first image in each specimen group is an normal SEM image of the structure. After this image the same position is also evaluated using EBSD (Electro BackScatter Diffraction).

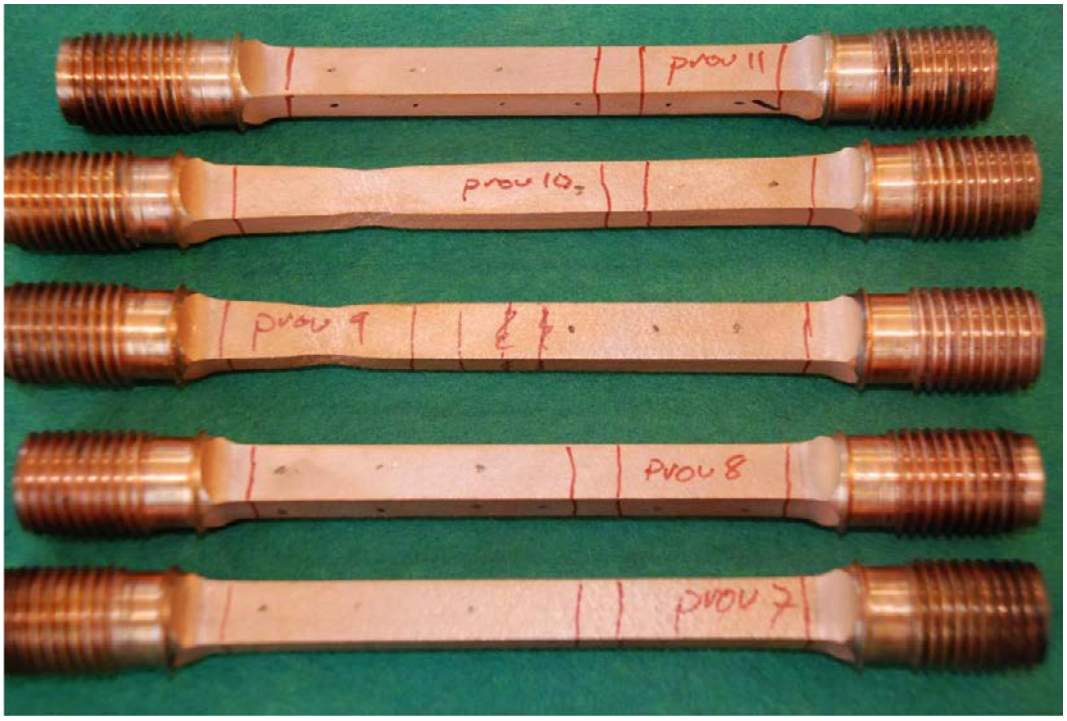

Figure 8-1. *The creep test specimens after testing. The pieces marked by the parallel red lines are the material extracted for metallography.*

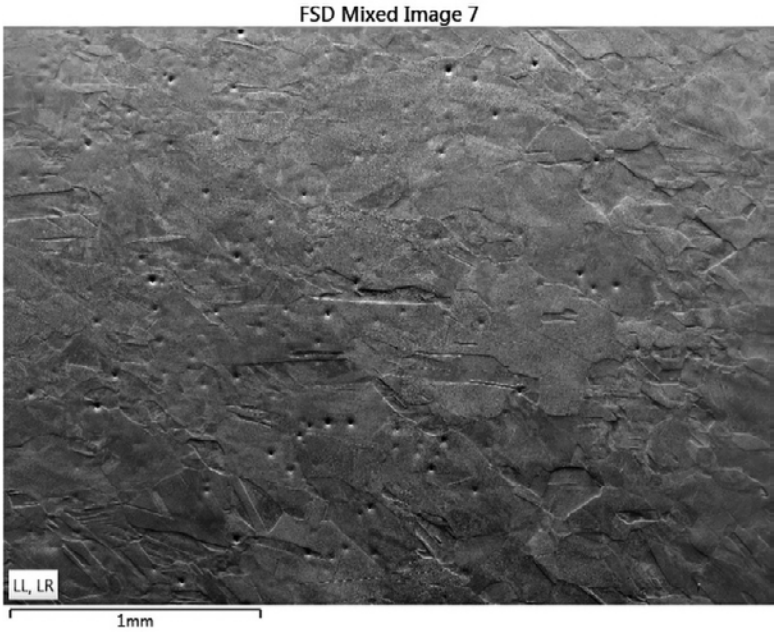

Figure 8-2. *SEM image from specimen 7.*

This method gives the ability to colour different grain orientations in different colours. In this way the grains are readily identifiable. The method also provides for identifying the mismatch between the grain orientations of two adjacent domains. This means grain boundaries and twin boundaries. The mismatch at a grain boundary can be any angle, but if the mismatch angle is exactly 60° in the (111)-direction it is a twin boundary in copper. In this way the microstructure can be assessed and measurements can be made. For instance the degree of recrystallization can be observed since recrystallized grains show up with a uniform colour without any gradations. The grain size spectrum can also be measured using the information in the EBSD.

In EBSD of annealed material the individual grains usually show up as one uniform colour. When a material is deformed, the internal structure within the grains is stretched which shows up as a gradual toning or patterning of the colour. The more deformation, the greater the change of the colour. In the images below it is evident that the deformation is greater in some grains than in others. This is not surprising since the grains with the most favourable orientation for deformation is those that will take up most of the deformation.

During manufacturing of the copper the heat treatments and the mechanical treatments to the material results in a microstructure consisting of roughly equiaxed grains with the occasional twin boundary pair through the grain. The twins develop when the internal stresses in the grain become too great and by twinning the stresses are relaxed. Such a twin is readily identifiable as just a twin from the appearance. In this study many of the twin boundaries visible in the images as twin boundaries, are in fact not in the creep tested material. They have been converted to regular grain boundaries by the rotation of the grains due to the creep deformation. In practice this is evident since the grain boundaries no longer have a mismatch of 60°.

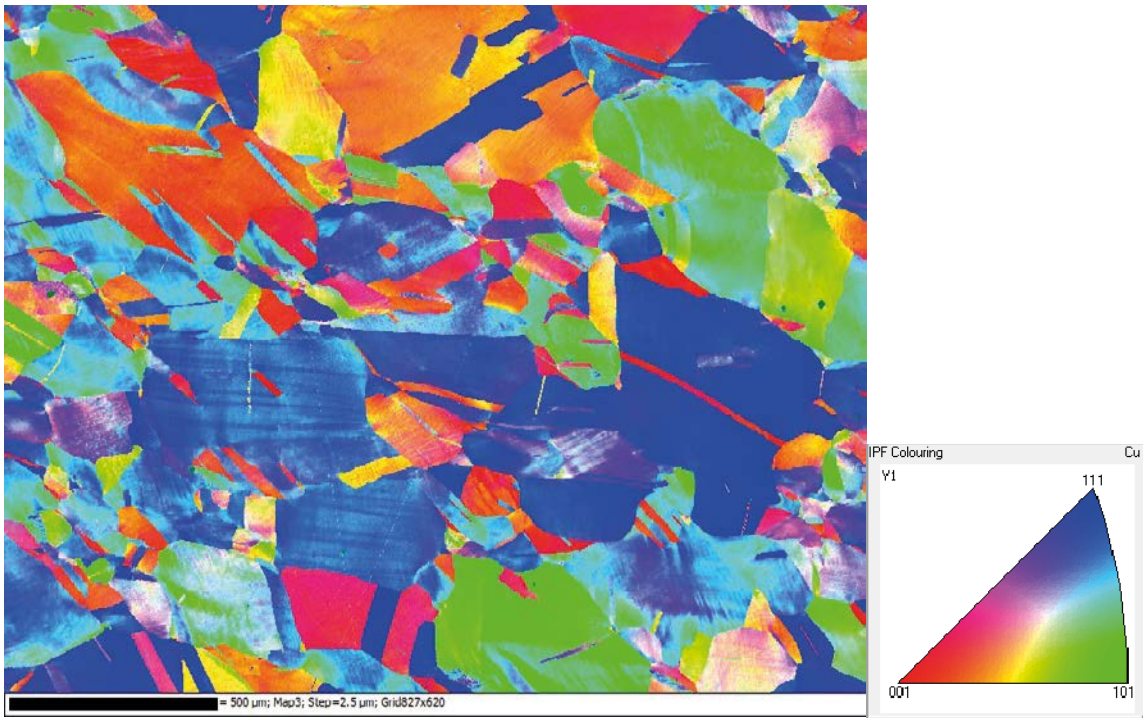

Figure 8-3. *Crystallographic orientation in specimen 7 using 2.5 µm step size. Same position as in Figure 8-2.*

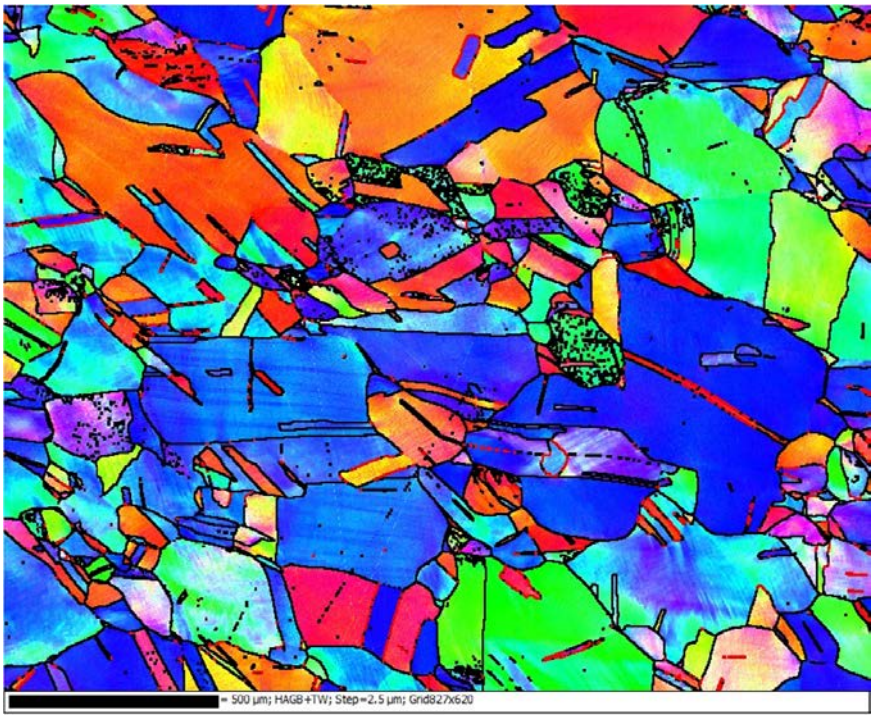

Figure 8-4. *High angle boundaries in specimen 7. Same position as in Figure 8-2.*

Figure 8-5. *SEM image from specimen 8.*

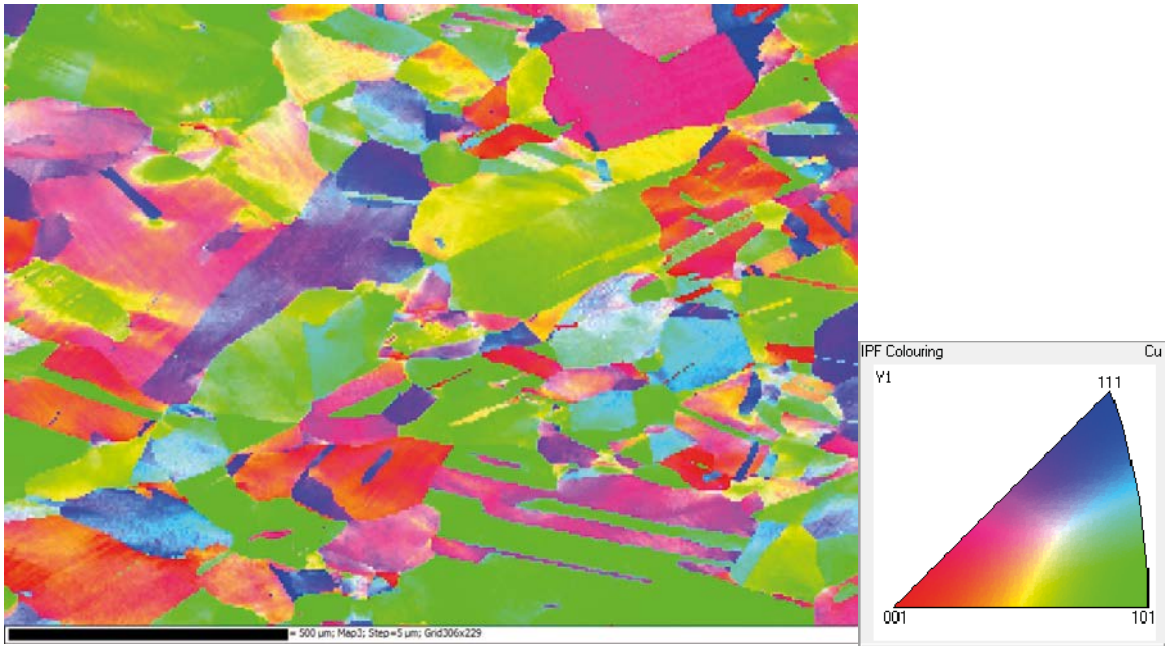

Figure 8-6. *Crystallographic orientation in specimen 8 using 2.5 µm step size. Same position as in Figure 8-5.*

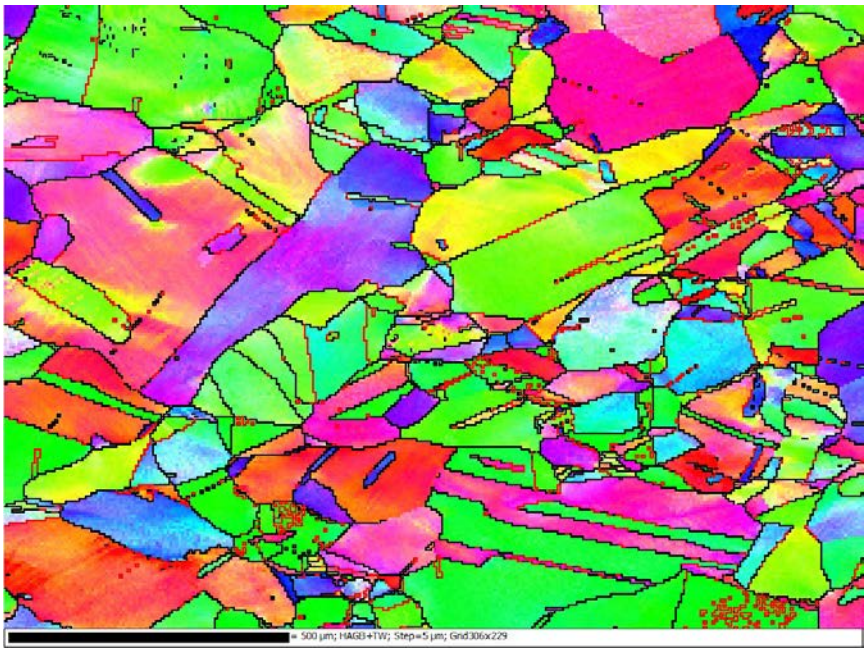

Figure 8-7. *High angle boundaries in specimen 8. Same position as in Figure 8-5.*

Figure 8-8. *SEM image from specimen 11.*

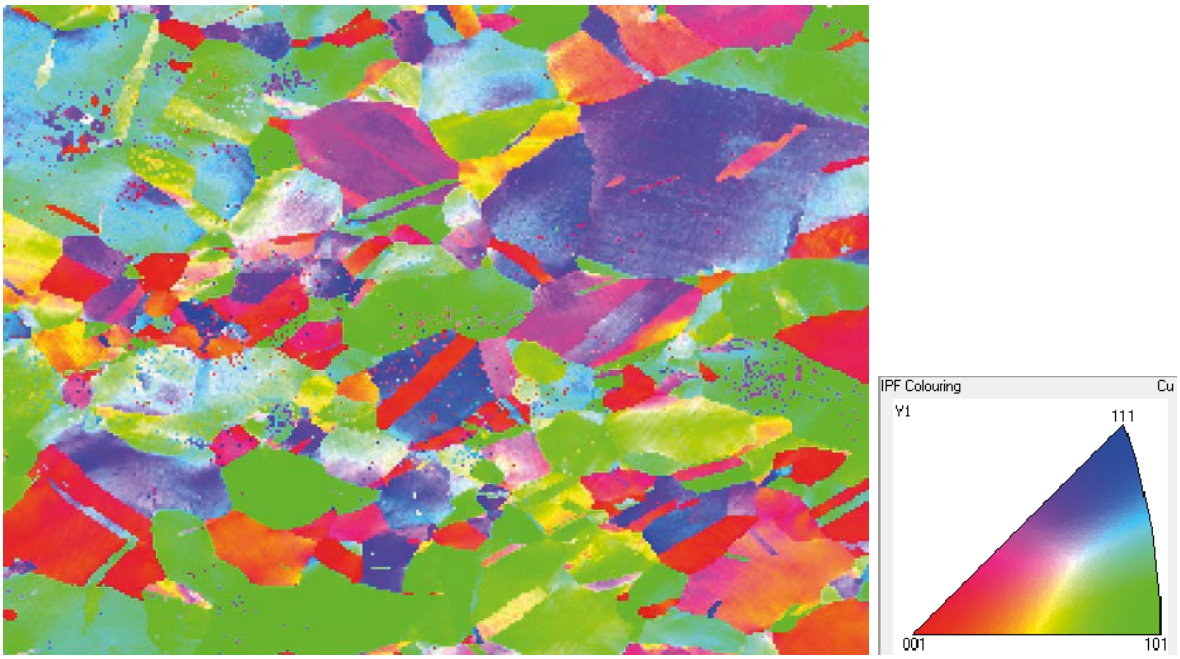

Figure 8-9. *Crystallographic orientation in specimen 11 using 2.5 µm step size. Same position as in Figure 8-8.*

Figure 8-10. *High angle boundaries (thick black) and low angle boundaries (thin black) in specimen 11. Low angle boundaries are associated with the grain substructure and the density is a measure of the strain in the grain.*

Specimens 7 through 11 was creep tested in this project and were all made from Cu-OFP. There is no obvious difference between the tested materials apart from a larger amount of deformation in those specimens tested to a longer creep strain. The colour in the grains are slightly multi-coloured, meaning that no grain recrystallization has taken place. The amount of twinning is similar in all tests.

The study of Cu-OF was also seen as interesting and material from an earlier creep test program on oxygen free copper was also included in the SEM study. The material had been creep tested at a similar temperature and time as the Cu-OFP (Andersson et al. (2013). The results show that the shape and appearance of the microstructure is roughly similar to Cu-OFP.

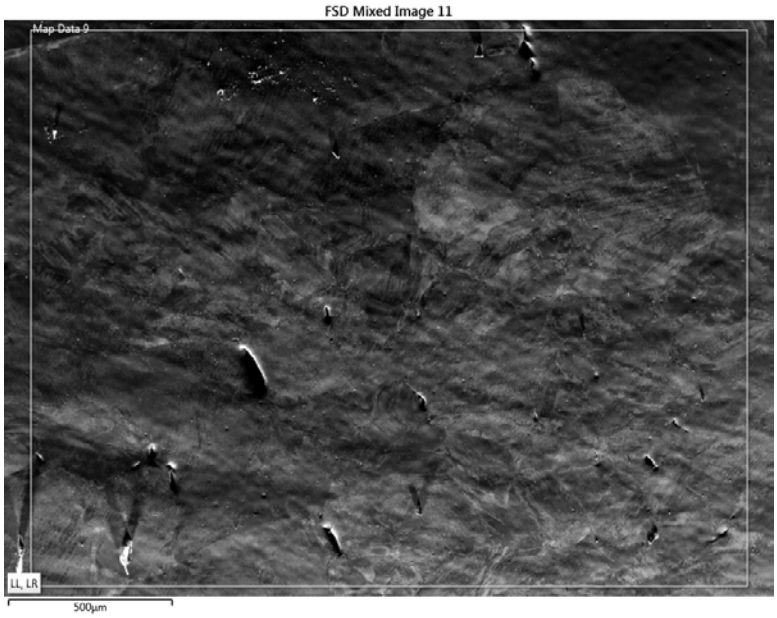

Figure 8-11. *SEM image from specimen 15-11. This specimen is made from Cu-OF from a previous creep test study.*

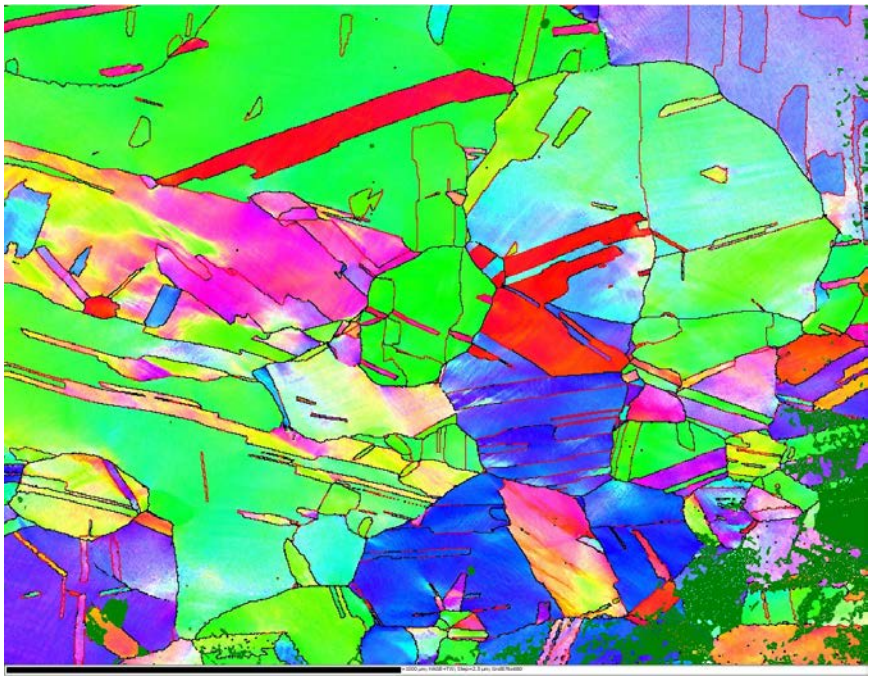

Figure 8-12. *Crystallographic orientation in specimen 15-11 using 2.5 µm step size. Same position as in Figure 8-11.*

EBSD can be performed using different step sizes. To cover a large area a large step size is used, as in the images above where the step size is 2.5–5 µm. When the step size is decreased more details in the individual grains are visible. In Figure 8-13 the step size is 0.1 µm. At this magnification the sub-structure in the grain interior is visible. The line scan marked b) shows that the grain has a gradual shift in mismatch along the line with the individual sub-grain boundaries showing up as peaks in the line. In line scan c) a large peak is visible which probably is a substructure developing into what might eventually be a twin.

a)

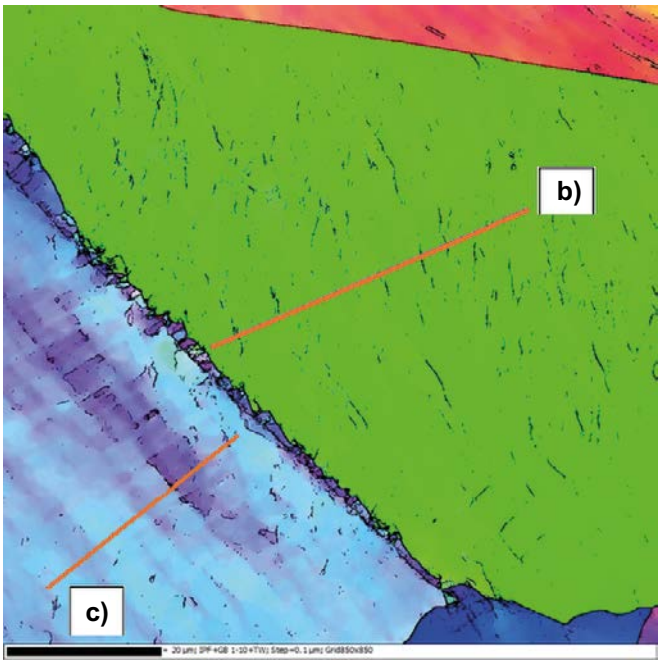

b)

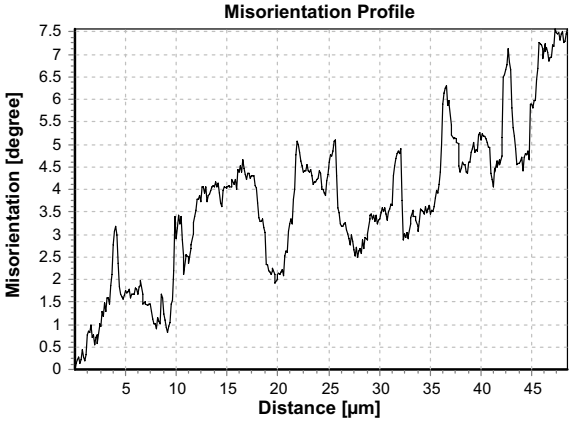

c)

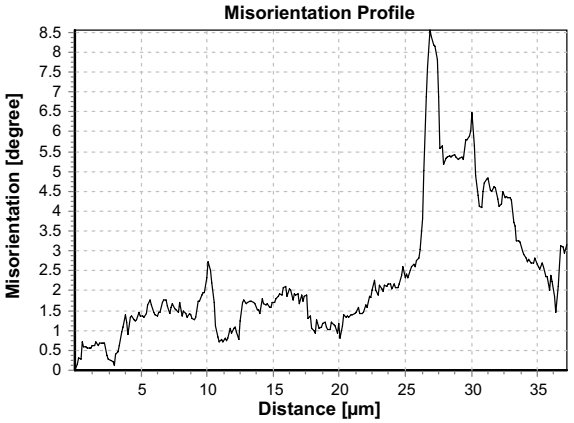

Figure 8-13. *High angle boundaries in specimen 15-11. Two linescans of the misalignment angle marked b) and c) in image a) are also given in b) and c). The peaks in the misalignment represent subgrain boundaries.*

8.3 TOF-SIMS

Experiments using Time-Of-Flight-Secondary Ion Mass Spectroscopy (TOF-SIMS) were performed using a world leading instrument in Germany. Previously it has proved difficult to locate the phosphorus atoms within the copper matrix. It has even been difficult to ascertain if the phosphorus has been concentrated to the grain boundaries, in solid solution in the interior of the grains or if it has been bound in phosphates within the material. The new instrument has proved useful in locating the phosphorus in actual copper samples.

The material used in the studies was from the HOSP studies (Wu and Sandström 2015). Three different materials were tested initially. One with high phosphorus content, one with low phosphorus content and one reference material with medium phosphorus content. The material chemical composition is given in Table 8-2. This material was selected to give a range of phosphorus contents to study.

Table 8-2. Desired and measured chemical compositions as well as grain size for test materials. From Wu and Sandström (2015).

Material	Dimension (mm)	Chemical composition	Hydrogen[1] (wt-ppm)	Oxygen (wt-ppm)	Sulphur (wt-ppm)	Phosphorus (wt-ppm)	Grain size (µm)
M1LP[2] 111025101	300 × 90 × 55 (approximately)	Desired	0.5–1	7–10	10–15	25–30	400–500
		Measured	0.48/0.64	6.8/7.1	11.6/11.7	32/33	200[3] 420[4]
M2HP[2] 111032101	300 × 90 × 55 (approximately)	Desired	0.5–1	7–10	10–15	110–115	400–500
		Measured	0.45/0.6	7/7.6	11.9/12.6	112/115	230[3] 600[4]
REF 111027101	330 × 120 × 50 (approximately)	Desired	< 0.4	3–5	3–7	55–65	100–200
		Measured	0.53/0.63	3.1/3.1	3/3	65/66	150[3]

[1] Hydrogen could not be added to more than about 0.6 ppm.

[2] Vacuum cast, hot forged under controlled conditions, and heat treated at 950 °C/45 min.

[3] Grain size after forging.

[4] Grain size after heat treatment.

In a TOF-SIMS study the secondary ion studied in a SEM is fed into a time of flight mass spectrometer. This analysis method is largely qualitative and not quantitative in nature. The number of counts depends on the number of ions being expelled from the surface of the material and some ions are easier to expel than others. It is not possible to measure an absolute phosphorus level in the material but it is possible to compare the levels of several measurements on the same sample, or different samples prepared in the same way and studied at the same time.

The materials above was sectioned, ground and polished in Germany. Care was taken during the preparation not to introduce any foreign materials in the copper and the final polish was done by electro-polishing. No etch was applied to the surface after polishing, but a light sputtering with Cs was applied to both clean the surface and increase the intensities of C, O, P and S. The analysis was performed by identifying the microstructure in SEM mode, positions for closer study were identified and the instrument then automatically analysed these positions. The positions were chosen as being inside both small and large grains and also close to the centre and close to the grain boundaries inside the grains. The aim of the study was to identify if a segregation of phosphorus existed within or between grains.

Examples of the results from the analysis are given in Figure 8-14 to Figure 8-16.

All studies performed in TOF-SIMS show similar results. The phosphorus content in the materials vary between the tested materials with the high phosphorus material having higher normalised content than either the low phosphorus or the REF material. There is no evidence of either a segregation of phosphorus to the grain boundaries, from the grain boundaries or inside the individual grains.

The phosphorus content is remarkably uniform for all tested areas, notwithstanding if the area is within a grain, a grain boundary or close to a grain boundary. In Figure 8-17 to Figure 8-19 the normalised intensities are compared for phosphorus, sulphur and oxygen for the three materials for three typical analysis positions. The sites chosen are large grains, small grains and grains called dark grains which shows up as dark coloured on SEM images. The dark grain do not have a significantly different chemical composition, but the darkness is probably connected with the grain orientation. There is no statistically significant difference in either phosphorus or sulphur for these positions within the same material (HP, LP or REF), but a small difference in oxygen for the dark grains.

Further studies on new delivered materials including a piece of the creep tested material from the creep test study reported above showed similar results, an example of the results are given in Figure 8-20 with the corresponding table of intensities in Figure 8-21.

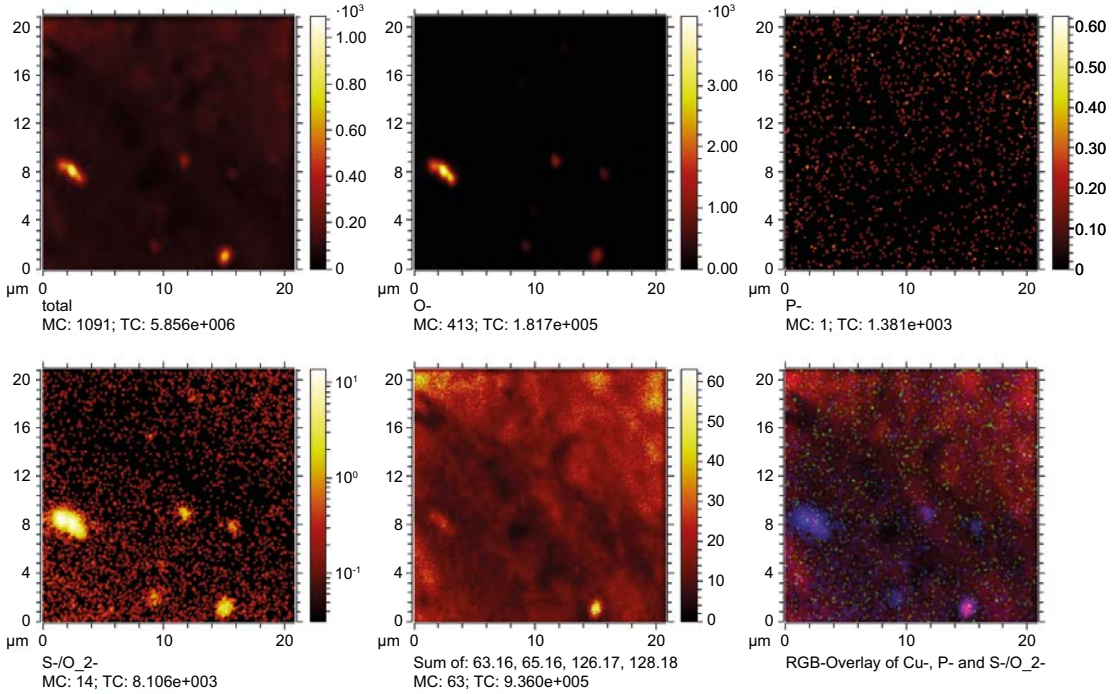

Figure 8-14. *TOF-SIMS mapping of chemical composition of a surface from the REF material. The images in the top row are: total, oxygen and phosphorus, bottom row: sulphur, all counts collected and an overlay of O, S and P mappings. Note that for oxygen and for sulphur both particles and grain boundaries are visible, for phosphorus neither.*

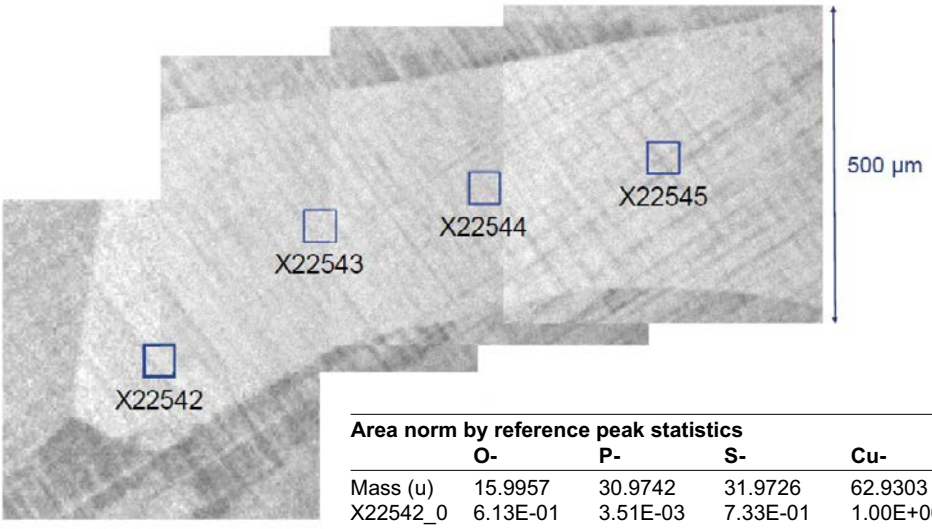

Area norm by reference peak statistics					
	O-	P-	S-	Cu-	Total counts
Mass (u)	15.9957	30.9742	31.9726	62.9303	
X22542_0	6.13E-01	3.51E-03	7.33E-01	1.00E+00	589223
X22543_0	1.17E+00	4.76E-03	2.22E+00	1.00E+00	974213
X22544_0	5.74E-01	5.73E-03	1.06E+00	1.00E+00	755626
X22545_0	1.26E+00	5.33E-03	4.69E-01	1.00E+00	1064199
Mean	9.05E-01	4.83E-03	1.12E+00	1.00E+00	
RSD (%)	3.46E+01	1.73E+01	5.96E+01	0.00E+00	

Figure 8-15. *TOF-SIMS analysis of a large grain from the high phosphorus material. The phosphorus content is almost similar in all measurement points.*

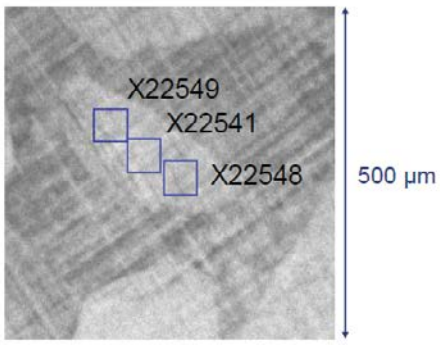

Area norm by reference peak statistics					
	O-	P-	S-	Cu-	Total counts
Mass (u)	15.9957	30.9748	31.9726	62.9303	
X22541_0	2.04E+00	5.74E-03	1.05E+00	1.00E+00	858421
X22548_0	7.84E-01	5.44E-03	1.54E+00	1.00E+00	1015359
X22549_0	6.22E-01	6.58E-03	1.49E+00	1.00E+00	1170492
Mean	1.15E+00	5.92E-03	1.36E+00	1.00E+00	
RSD (%)	5.51E+01	8.11E+00	1.63E+01	0.00E+00	

Figure 8-16. *TOF-SIMS analysis of a small grain from the high phosphorus material. The phosphorus content is almost similar in all measurement points.*

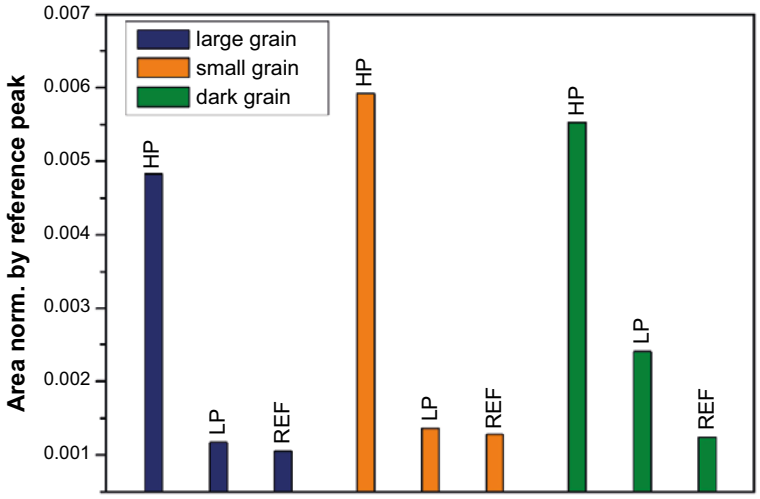

Figure 8-17. *TOF-SIMS analysis of the phosphorus content the three materials. Note that the high phosphorus material (HP) has a higher content of phosphorus than the low phosphorus material (LP) and the reference material. Dark grains refer to a set of grains that shows up dark on the SEM images.*

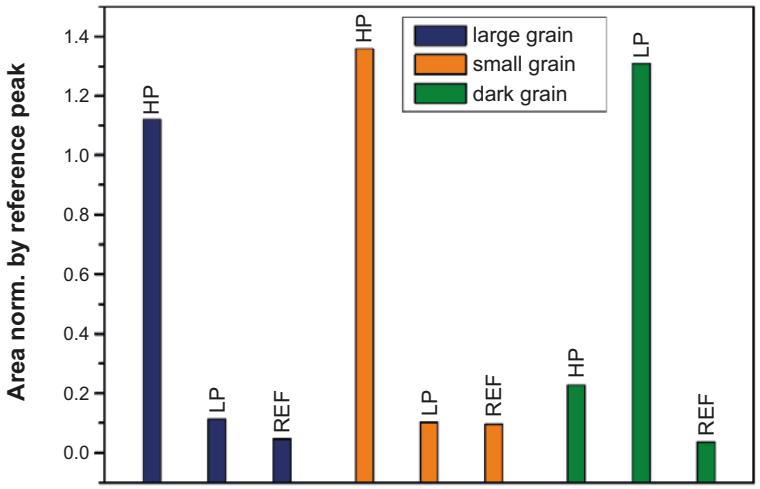

Figure 8-18. *TOF-SIMS analysis of the sulphur content the three materials. Dark grains refer to a set of grains that shows up dark on the SEM images.*

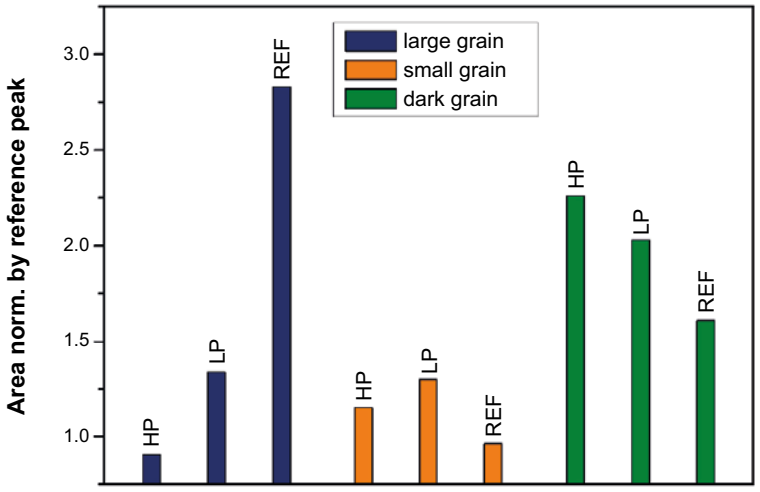

Figure 8-19. *TOF-SIMS analysis of the oxygen content the three materials. Note that the dark coloured grains apparently have higher oxygen content. Also that there seems to be a segregation of oxygen to large grains in the REF material.*

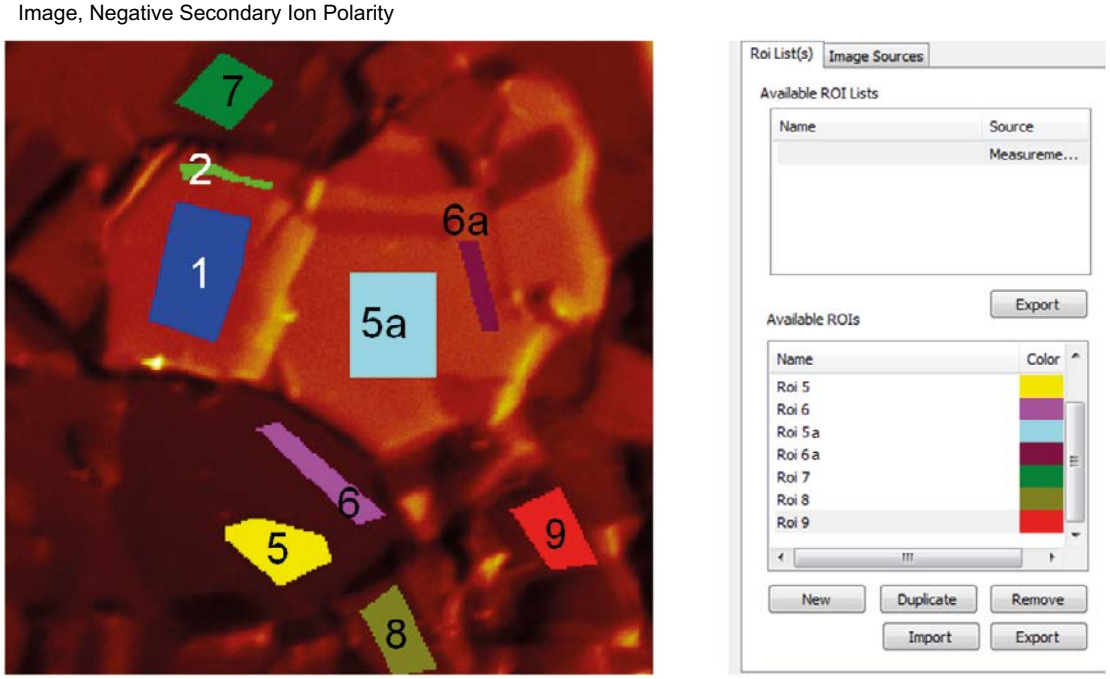

Figure 8-20. *An example of the evaluation of different sites in a copper microstructure of the REF material. Different regions of interest (roi) are identified and has been studied by TOF-SIMS.*

Negative secondary ion polarity - Normalised intensities

	Mass (u)	_Roi 1 A30955	_Roi 2 A30955	_Roi 5 A30955	_Roi 6 A30955	_Roi 5 (a) A30955	_Roi 6 (a) A30955	_Roi 7 A30955	_Roi 8 A30955	_Roi 9 A30955
C-	**12**	0.90 %	0.95 %	0.27 %	0.32 %	0.65 %	0.64 %	0.33 %	0.46 %	0.30 %
O-	**16**	2.33 %	2.65 %	3.13 %	2.72 %	1.44 %	1.33 %	3.85 %	3.60 %	3.87 %
P-	**31**	0.09 %	0.14 %	0.16 %	0.16 %	0.09 %	0.07 %	0.12 %	0.17 %	0.16 %
S-	**32**	0.38 %	0.40 %	0.35 %	0.28 %	0.20 %	0.21 %	0.47 %	0.31 %	0.57 %
Cu-	**63**	224.00 %	224.00 %	223.00 %	223.00 %	223.00 %	223.00 %	223.00 %	223.00 %	220.00 %
^65Cu-	**65**	100.00 %	100.00 %	100.00 %	100.00 %	100.00 %	100.00 %	100.00 %	100.00 %	100.00 %

Table 1:
Normalised intensities I/I(^{65}Cu) of selected ions in negative secondary ion polarity; data in %

Figure 8-21. *The evaluation of the normalised intensities of the chemical elements in Figure 8-20. Note that the amount of phosphorus is the same for all regions of interest.*

8.4 Annealing experiments on Cu-OFP

Annealing experiments on Cu-OFP has been performed in another study (Taxén et al. 2018). The main intention here was to replicate stress corrosion cracking results from a Japanese study (Taniguchi and Kawasaki 2008) using SKB copper. Copper was annealed fully and then subjected to cold rolling to maximise the cold working and the material hardness. Out of this material several pieces was then cut and annealed at different temperatures and different times to produce a material with the same hardness as the Japanese material. Annealing was in a salt bath using a commercial mix of sodium nitrite and sodium nitrate followed by subsequent immediate water quenching. Since the results would also be of interest to the phosphorus work the test matrix was a little extended to more temperatures and times than was needed just for the stress corrosion cracking study. The results can be found in Figure 8-22. The results show how 5 minutes annealing affects the hardness at the higher temperatures and that the effect of the annealing disappears gradually at temperatures below 400 °C. The same experiments were performed at 10 minutes annealing where there is a sharp decrease in the annealing efficiency between 400 and 375 °C. Since recrystallization of copper grains is limited or non-existent at these annealing temperatures and times, the whole effect must be down to subgrain dissolving and rearrangement. This in turn is dependent on the dislocation mobility, which is decreased as the temperature is decreased. Studies of the dislocation and subgrain development

support this (Sandström 1977). While these results cannot be directly applied to creep testing at temperatures of 75–100 °C, the indication is that the subgrain structure is quite robust at higher temperatures and should be even more so at the lower temperatures of the repository.

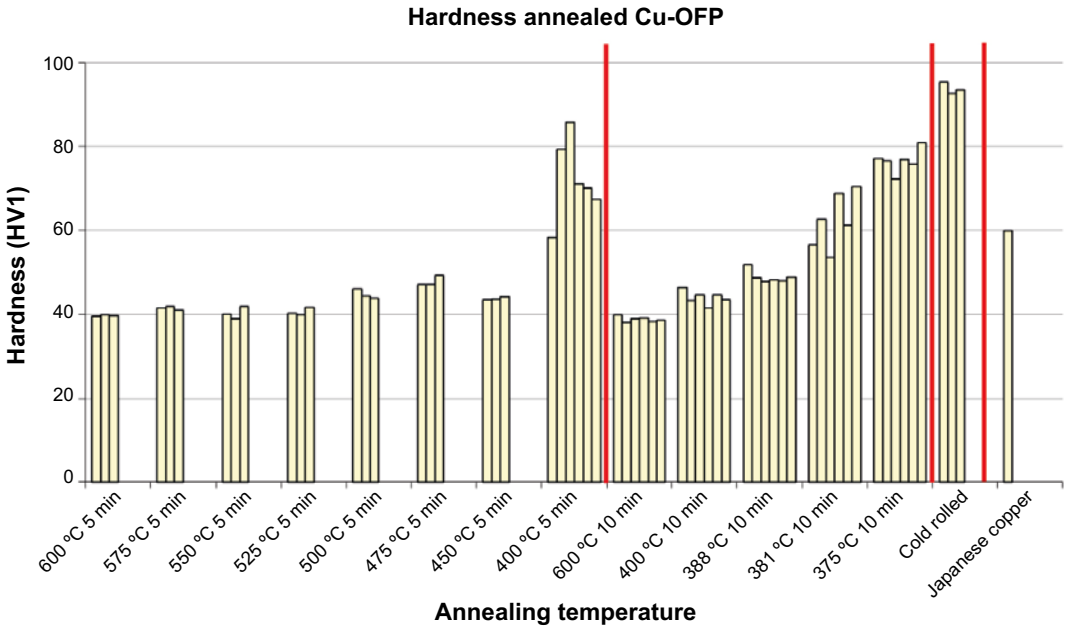

Figure 8-22. *Hardness in Cu-OFP after annealing, cold working and then re-annealing, The first part is copper annealed at different temperatures for 5 minutes, the second part is the same copper annealed for 10 minutes at different temperatures, the third part is the hardness as cold rolled and the last part the Japanese hardness. Each vertical bar represents one experiment. From Taxén et al. (2018).*

9 Discussion

9.1 Microstructural modelling and relaxation experiments

The results of the study presented in this report are preliminary. The objective of the microstructural modelling and related tensile experiments was to examine whether any microstructural differences between Cu-OF and Cu-OFP could be observed that could aid in understanding the effect of added phosphorus on the mechanical properties of copper. Observations from this study are:

- As expected, EBSD is effective in finding recrystallized grains in a microstructure.
- That the addition of 50 ppm phosphorus to Cu-OF suppresses recrystallization.
- That heat treatment of cold worked specimens of Cu-OF promotes recrystallization.
- As previous experience shows the amount of recrystallization increases with increasing temperature for the heat treatment.

The results obtained in this study are too few to understand the effect of adding phosphorus to Cu-OF on the tendency for recrystallization.

9.2 Grain size distribution modelling

Two models of polycrystalline microstructures were analysed. The first model was comprised of a uniform size distribution of grains, and the second model was comprised of a bimodal grain size distribution with small grains and large grains, the latter being approximately ten times larger by area than the former. Based on microscopy images, it has been suggested that in a bimodal grain structure, there is a tendency for smaller grains to accommodate disproportionately high levels of deformation compared to large strains. Modelling has shown that macroscopic deformation is accommodated in the material through a distribution of local shear bands. There is no observable effect of a bimodal grain structure on the local deformation behaviour of the microstructure. There is no significant difference between large and small grains in their respective contributions to the overall deformation of the material. Furthermore if the Petch-Hall grain size effect had been included in the constitutive description of the material, it is likely that smaller grains would have deformed less than large grains, as smaller grains would have been harder than large grains.

9.3 Diffusion dynamics in Cu-OFP

Magnusson and Frisk (2013) discussed the dynamics of phosphorus atom movement in a copper matrix. They found that the movement of phosphorus atoms in copper is nearly negligible at low temperatures. There is a slight possibility for movement of phosphorus atoms at grain boundaries. This is assessed as up to 5 cm per 100 000 years at 40 °C. They have also found that since phosphorus has a high solubility in copper, almost no copper phosphates will form during manufacturing of the copper.

9.4 Phosphorus distribution in Cu-OFP

The TOF-SIMS studies have shown that there is no visible segregation of phosphorus to either the grain boundaries or from the grain boundaries. Neither is there any evidence of a systematical variation of the phosphorus content within the grains. Further, no phosphates or other phosphorus containing particles have been observed. The most probable conclusion is that all of the phosphorus is held in solid solution in the copper matrix as individual atoms or at most as congregates of atoms.

There may be a monolayer of atoms decorating grain boundaries, a monolayer would be difficult to detect using the current analysis methods, but there are no indications of this from the TOF-SIMS results. Ab initio calculations of phosphorus atoms in a copper matrix are needed to fully illuminate the behaviour of individual copper atoms in the presence of vacancies, stacking faults or grain boundaries.

9.5 Grain boundary stability and recrystallization

The grain structure of copper is found to be stable at temperatures lower than that used for annealing work. The annealing study shows that for even partial annealing, and thus the resolution of the dislocation substructure, a temperature of at least 375 °C is needed at short times. For recrystallization even longer times or higher temperatures are needed. In the studied creep tests no evidence of recrystallization is visible at 75 °C/188 hours, which is in accordance with previous results, and indeed with the findings from the microstructural modelling and the related tensile tests. Instead the larger creep strain in the specimens with larger strain is taken up by more deformation of individual grains. This would provide the driving force for recrystallization, had the temperature been high enough, but at the results show that this has not happened.

A literature study has not showed any studies of recrystallization on bulk copper materials at room temperature and slightly above. Studies of stabilised fatigue cycles of copper usually do not mention any observations of recrystallization taking place (Jiang et al. 2015).

9.6 Creep in phosphorus containing copper

Creep in copper is the movement of dislocations in the material leading to a macroscopical deformation. The movement of the dislocation is influenced of the driving force which is the applied stress, and the obstacles for movement. Cu-OFP is a homogenous material with few foreign structures, which means that the obstacles are grain boundaries, solute atoms, particles if present and finally other dislocations. Very few foreign particles have ever been found in Cu-OFP outside welds that might be decorated by oxide bands and they are hereafter neglected.

TEM studies has shown that the dislocations in the copper form substructures in the grains (Wu et al. 2014). These substructures depend on the amount of creep and also on the amount of obstacles the dislocations encounter. More creep deformation leads to finer subgrain structures and also to thicker subgrain boundaries. The subgrain boundary consists of stacked dislocation bands. The interaction between the creep deformation and the subgrain structure has been studied for Cu-OFP (Sandström 2016).

Solute atoms create a Cottrell atmosphere around themselves. This atmosphere is an elastic distortion of the lattice surrounding the interstitial or substitutional atom. The atmosphere traps and hinders a moving dislocation that comes into contact with it. The interaction between the Cottrell atmospheres and the dislocations is what decides the shape of the subgrain structure along with outer factors such as grain boundaries and twin boundaries.

The conclusion if all of the above is taken into consideration is that the structure the dislocations move through is constant over time, as phosphorus and grain boundaries do not move. Following from this the creep properties should also be constant over time. Thus a property shown to be experimentally valid at shorter times up to a few years, should still be present at very long timescales.

9.7 The role of phosphorus in the creep of Cu-OFP

The main aim of this work has been to study the role of phosphorus in the development of creep in phosphorus containing copper. It has not during the work been possible to determine the exact mechanism of how phosphorus increases the creep ductility. Instead it has been possible to prove that phosphorus is evenly distributed in the material and not significantly segregated to grain boundaries

or bound in particles like phosphates. Phosphorus is most probably in solid solution in the copper grains. A recent study (Magnusson and Frisk 2013) have also shown that these phosphorus atoms will not move over the time of the repository, meaning that the effects of the phosphorus atoms on the creep dislocation movement should be constant.

Furthermore, studies of the grain boundaries and recrystallization indicate that no movement of grain boundaries is likely during the repository. The microstructure in which the creep takes place is thus assessed as being constant during the repository, and so are the creep properties.

9.8 Questions raised by the work in this report

The recrystallization behaviour of copper at temperatures relevant for the repository are not fully investigated. The work presented in this report indicates that recrystallization will not take place, but more studies at lower temperatures are needed to verify the indications.

While the studies in this work have indicated an even distribution of phosphorus atoms in the copper matrix, the presence of a monolayer at the grain boundaries cannot be excluded. This needs further clarification, and the possible way is more spectroscopy studies, like Auger spectroscopy on fracture surfaces.

Further studies of Cu-OF to evaluate the effect of phosphorus free copper compared to non-phosphorus containing copper are also needed It is not fully known if the effects shown for Cu-OFP is dependant of the phosphorus content or if the way the testing is performed also affected the results. The method of testing has developed greatly since the previous Cu-OF testing.

10 Conclusions

Cu-OFP has been extensively modelled and also creep tested at 75 °C. The work has provided the following conclusions:

- That the addition of 50 ppm phosphorus to Cu-OF suppresses recrystallization.
- That heat treatment of cold worked specimens of Cu-OF promotes recrystallization.
- That the amount of recrystallization increases with increasing temperature for the heat treatment.
- There is no observable effect of a bimodal grain structure on the local deformation behaviour of the microstructure.
- There is no significant difference between large and small grains in their respective contributions to the overall deformation of the material.
- EBSD performed on the material after testing show that no recrystallization has taken place in the material during creep testing.
- TOF-SIMS studies show that the phosphorus content is evenly spaced in the material within the grains and not segregated to either particles or any structures.
- Annealing experiments has shown that the annealing of the dislocation substructure is time and temperature dependent, and that at least 375 °C are needed to affect the structure in 10 minutes annealing time, confirming the relaxation experiments.
- Microstructural modelling and relaxation experiments indicate that no recrystallization is anticipated at the low temperatures.
- Creep by dislocation movement is dependent on the amount of obstacles the dislocation encounters. The work in this report has shown that the obstacles in the copper material (phosphorus atoms, grain boundaries) are constant over time and that the creep properties should also remain constant over long and short timescales.

References

SKB's (Svensk Kärnbränslehantering AB) publications can be found at www.skb.com/publications. SKBdoc documents will be submitted upon request to document@skb.se.

ABAQUS, 2014. Dassault Systèmes Simulia Corp., Providence, Rhode Island.

Adriaens A, Van Vaeck L, Adams F, 1999. Static secondary ion mass spectrometry (S-SIMS) Part 2: material science applications. Mass Spectrometry Reviews 18, 48–81.

Andersson-Östling H C M, Sandström R, 2009. Survey of creep properties of copper intended for nuclear waste disposal. SKB TR-09-32, Svensk Kärnbränslehantering AB.

Andersson H, Sandström R, Seitisleam F, 2013. Influence of phosphorous and sulphur as well as grain size on creep in pure copper. SKB TR-99-39, Svensk Kärnbränslehantering AB.

Benninghoven A, 1994. Chemical analysis of inorganic and organic surfaces and thin films by static time-of-flight secondary ion mass spectrometry (ToF-SIMS). Angewandte Chemie International 33, 1023–1043.

Gurtin M E, Fried E, Anand L, 2010. The mechanics and thermodynamics of continua. New York: Cambridge University Press.

Henderson P J, Sandström R, 1998. Low temperature creep ductility of OFHC copper. Materials Science and Engineering A 246, 143–150.

Jiang J, Britton T B, Wilkinson A J, 2015. Evolution of intragranular stresses and dislocation densities during cyclic deformation of polycrystalline copper. Acta Materialia 94, 193–204.

Kalidindi S R, 1992. Polycrystal plasticity: constitutive modeling and deformation processing. PhD thesis. Massachusetts Institute of Technology.

Korzhavyi P A, Abrikosov I A, Johansson B, 1999. Theoretical investigation of sulfur solubility in pure copper and dilute copper-based alloys. Acta Materialia 47, 1417–1424.

Magnusson H, Frisk K, 2013. Self-diffusion and impurity diffusion of hydrogen, oxygen, sulphur and phosphorus in copper. SKB TR-13-24, Svensk Kärnbränslehantering AB.

Magnusson H, Frisk K, 2014. Thermodynamic evaluation of the copper-rich part of the Cu–H–O–S–P system at lower temperatures. CALPHAD 47, 148–160.

Mannesson K, Andersson-Östling H C M, 2013. Creep of copper with different NDT sound attenuation. Swerea KIMAB AB, Sweden. SKBdoc 1411196. ver 1.0, Svensk Kärnbränslehantering AB.

Mannesson K, Andersson-Östling H C M, Sandström R, 2013. Influence of local cold work in creep failure of phosphorus doped oxygen free copper. SKB R-13-32, Svensk Kärnbränslehantering AB.

Modin S, Modin H, 1985. Handbok i metallmikroskopering. 4th ed. Årsta: Meritförlaget. (In Swedish.)

Pettersson K, 2012. A review of the creep ductility of copper for nuclear waste canister application. Technical Note 2012:13, Strålsäkerhetsmyndigheten (Swedish Radiation Safety Authority).

Pettersson K, 2016. An updated review of the creep ductility of copper including the effect of phosphorus. Report 2016:02, Strålsäkerhetsmyndigheten (Swedish Radiation Safety Authority).

Quey R, 2014. Neper reference manual: the documentation for Neper 3.1.1, a software package for polycrystal generation and meshing. Available at: http://neper.sourceforge.net/docs/neper.pdf

Quey R, Dawson P R, Barbe F, 2011. Large-scale 3D random polycrystals for the finite element method: Generation, meshing and remeshing. Computer Methods in Applied Mechanics and Engineering 200, 1729–1745.

Raiko H, Sandström R, Rydén H, Johansson M, 2010. Design analysis report for the canister. SKB TR-10-28, Svensk Kärnbränslehantering AB.

Sandström R, 1977. Subgrain growth occurring by boundary migration. Acta Metallurgica 25, 905–911.

Sandström R, 1999. Extrapolation of creep strain data for pure copper. Journal of Testing and Evaluation 27, 31–35.

Sandström R, 2014. The role of phosphorus for mechanical properties in copper. SKBdoc 1417069 ver 1.0, Svensk Kärnbränslehantering AB.

Sandström R, 2016. The role of cell structure during creep of cold worked copper. Materials Science and Engineering A 674, 318–327.

SKB, 2006. Kapsel för använt kärnbränsle. Konstruktionsförutsättningar. SKB R-06-02, Svensk Kärnbränslehantering AB. (In Swedish.)

SKB, 2010a. Design, production and initial state of the canister. SKB TR-10-14, Svensk Kärnbränslehantering AB.

SKB, 2010b. Design and production of the KBS-3 repository. SKB TR-10-12, Svensk Kärnbränslehantering AB.

SSM, 2014. Granskning och utvärdering av SKB:s redovisning av Fud-program 2013. Rapport 2014:12, Strålsäkerhetsmyndigheten (Swedish Radiation Safety Authority). (In Swedish.)

Taniguchi N, Kawasaki M, 2008. Influence of sulfide concentration on the corrosion behavior of pure copper in synthetic seawater. Journal of Nuclear Materials 379, 154–161.

Taxén C, Flyg J, Bergqvist H, 2018. Stress corrosion testing of copper in sulfide solutions. SKB TR-17-16, Svensk Kärnbränslehantering AB.

Van Vaeck L, Adriaens A, Gijbels R, 1999. Static secondary ion mass spectrometry (S-SIMS) Part 1: Methodology and structural interpretation. Mass Spectrometry Reviews 18, 1–47.

Wu R, Sandström R, 2015. Effect of phosphorus content on creep properties of Cu-OFP at 75 and 125 °C. KIMAB 2015-102, Swerea KIMAB AB, SKBdoc 1449099 ver 1.0, Svensk Kärnbränslehantering AB.

Wu R, Pettersson N, Martinsson Å, Sandström R, 2014. Cell structure in cold worked and creep deformed phosphorus alloyed copper. Materials Characterization 90, 21–30.

Arkitektkopia AB, Bromma, 2018

SKB is responsible for managing spent nuclear fuel and radioactive waste produced by the Swedish nuclear power plants such that man and the environment are protected in the near and distant future.

skb.se